

1 **Misfolded proteins bind and activate death receptor 5 to trigger apoptosis during**  
2 **unresolved endoplasmic reticulum stress**

3

4 **Authors:** Mable Lam<sup>1,2</sup>, Scot Marsters<sup>3</sup>, Avi Ashkenazi<sup>3,\*</sup>, and Peter Walter<sup>1,2,\*</sup>

5 **Affiliations:**

6 <sup>1</sup> Howard Hughes Medical Institute and Department of Biochemistry and Biophysics, University  
7 of California at San Francisco, CA, USA

8 <sup>2</sup> Department of Biochemistry and Biophysics, University of California at San Francisco, San  
9 Francisco, CA 94158, USA.

10 <sup>3</sup> Cancer Immunology, Genentech, Inc. 1 DNA Way South San Francisco, CA 94080, USA.

11 \* Corresponding author. E-mail: peter@walterlab.ucsf.edu (P.W.); aa@gene.com (A.A.)

12

13 **Abstract**

14 Disruption of protein folding in the endoplasmic reticulum (ER) activates the unfolded protein  
15 response (UPR)—a signaling network that ultimately determines cell fate. Initially, UPR  
16 signaling aims at cytoprotection and restoration of ER homeostasis; that failing, it drives  
17 apoptotic cell death. ER stress initiates apoptosis through intracellular activation of death  
18 receptor 5 (DR5) independent of its canonical extracellular ligand TRAIL; however, the  
19 mechanism underlying DR5 activation is unknown. In cultured human cells, we find that  
20 misfolded proteins can directly engage with DR5 in the ER-Golgi intermediate compartment,  
21 where DR5 assembles pro-apoptotic caspase 8-activating complexes. Moreover, peptides used  
22 as a proxy for exposed misfolded protein chains selectively bind to the purified DR5 ectodomain  
23 and induce its oligomerization. These findings indicate that misfolded proteins can act as  
24 ligands to activate DR5 intracellularly and promote apoptosis. We propose a model in which  
25 cells use DR5 as a terminal protein-folding checkpoint before committing to a terminal apoptotic  
26 fate.

## 27 **Introduction**

28           Proper folding of transmembrane and secreted proteins is critical to cell function and  
29 intercellular communication. Quality control of protein folding begins in the endoplasmic  
30 reticulum (ER) and responds to increased protein-folding demand during physiological or  
31 pathophysiological stresses. Accumulation of unfolded or misfolded proteins in the ER, known  
32 as ER stress, activates the unfolded protein response (UPR) – a network of intracellular  
33 signaling pathways that initially mount a cytoprotective response to restore ER homeostasis but  
34 can ultimately switch to a pro-apoptotic program under irresolvable stress (Walter and Ron  
35 2011; Tabas and Ron 2011). Two key UPR sensors, IRE1 and PERK coordinate the decision  
36 between cell survival and death through the delayed upregulation of the apoptosis-initiating  
37 protein death receptor 5 (DR5) (Lu et al. 2014; Chang et al. 2018).

38           During ER stress, IRE1 and PERK oligomerize upon directly binding to misfolded  
39 proteins, leading to their activation (Karagöz et al. 2017; Wang et al. 2018). PERK activation  
40 causes the selective translation of ATF4 and CHOP, which, in addition to upregulating genes  
41 that enhance the folding capacity of the ER, promotes the transcription of pro-apoptotic DR5  
42 (Harding et al. 2003; Yamaguchi and Wang 2004). The pro-apoptotic signal is initially  
43 counteracted by regulated IRE1-dependent mRNA decay (RIDD) that degrades DR5 mRNA (Lu  
44 et al. 2014). Upon prolonged ER stress, PERK exerts negative feedback on IRE1 activity  
45 attenuating RIDD, thus de-repressing DR5 synthesis to drive cell commitment to apoptosis  
46 (Chang et al. 2018).

47           DR5 is a pro-apoptotic member of the tumor necrosis factor receptor (TNFR) superfamily  
48 that signals from the plasma membrane into the cell in response to extracellular cues (Sheridan  
49 et al. 1997; Walczak et al. 1997; A Ashkenazi and Dixit 1998). It is constitutively expressed in  
50 various tissue types and forms auto-inhibited dimers in its resting state, analogous to other  
51 members of the TNFR family (Spierings et al. 2004; Pan et al. 2019; Vanamee and Faustman  
52 2018). In its canonical mode of activation, binding of the homotrimeric extracellular ligand TRAIL

53 (also known as Apo2L) (Wiley et al. 1995; Pitti et al. 1996) assembles DR5 into higher-order  
54 oligomers (Hymowitz et al. 1999; Mongkolsapaya et al. 1999; Valley et al. 2012). Consequently,  
55 DR5 forms intracellular scaffolds in which its cytosolic death domains recruit the adaptor protein  
56 FADD and pro-caspase 8 into the “death-inducing signaling complex” (DISC) (Kischkel et al.  
57 2000; Sprick et al. 2000; Jin et al. 2009; Dickens et al. 2012). Upon DISC-mediated  
58 dimerization, pro-caspase 8 molecules undergo regulated auto-proteolysis to form active  
59 initiator caspase 8 (Muzio et al. 1998). Activated caspase 8 frequently induces the intrinsic  
60 mitochondrial apoptotic pathway by truncating Bid, a pro-apoptotic Bcl2 protein, to cause Bax-  
61 mediated permeabilization of the mitochondrial outer membrane (Wei et al. 2001; LeBlanc et al.  
62 2002).

63 While DR5 and caspase 8 are both required for apoptosis during ER stress, we (Lu et al.  
64 2014; Lam et al. 2018), along with other independent groups, found unexpectedly that TRAIL is  
65 dispensable for this DR5 activation (Cazanave et al. 2011; Iurlaro et al. 2017; Dufour et al.  
66 2017). Indeed, upon ER stress, most newly synthesized DR5 molecules never make it to the  
67 plasma membrane but remain intracellular and thus inaccessible to extracellular ligands (Lu et  
68 al. 2014; Iurlaro et al. 2017). Given that at physiological levels DR5 is auto-inhibited until  
69 activated by a ligand, it remained a mystery how DR5 is activated in response to ER stress,  
70 prompting us to interrogate its intracellular mechanism of activation.

71

## 72 **Results**

73 *Misfolded proteins induce DR5-dependent apoptosis and can assemble DR5-caspase 8*  
74 *signaling complexes.*

75 To examine the mechanism of cell death driven by an unmitigated protein folding  
76 burden, we induced the exogenous expression of a GFP-tagged form of the glycoprotein myelin  
77 protein zero (MPZ) in epithelial cells (Fig 1A). MPZ initially folds in the ER and then travels to  
78 the plasma membrane to mediate membrane adhesion in myelin-forming Schwann cells, where

79 it is normally expressed. Mutations of MPZ that impair folding and cause its intracellular  
80 retention activate the UPR, leading to apoptosis in a manner dependent on CHOP (Pennuto et  
81 al. 2008). We found that in epithelial cells, titration of even non-mutant, GFP-tagged MPZ to  
82 high expression levels resulted in its intracellular accumulation, indicating a compromised MPZ  
83 folding state (Fig 1A). Folding-compromised MPZ induced a dose-dependent upregulation of the  
84 UPR transcriptional target genes CHOP, BiP, and DR5 (Fig 1–figure supplement 1A).  
85 Upregulated DR5 was retained intracellularly (Fig 1A, Fig 1–figure supplement 1B) and occurred  
86 concomitantly with cleavage of caspase 8 and its downstream target caspase 3 (Fig 1B). By  
87 contrast, low levels of MPZ-GFP expression that exhibited proper plasma membrane  
88 localization did not induce caspase 8 or 3 activity (Fig 1A-1B). To determine when caspase 8  
89 became active relative to cytoprotective UPR signaling, we assessed IRE1 activity during high  
90 MPZ-GFP expression through analysis of *XBP1* mRNA splicing. As expected, IRE1-mediated  
91 *XBP1* mRNA splicing initiated a few hours post-transfection with MPZ-GFP and later attenuated  
92 (Fig 1–figure supplement 1C). The upregulation of DR5, caspase activity, and PARP cleavage  
93 (another indicator of apoptotic progression) occurred after the attenuation of IRE1 activity,  
94 consistent with the hallmarks of terminal pro-apoptotic UPR signaling (Fig 1–figure supplement  
95 1D-1E).

96 To determine if DR5 was required for apoptosis during this sustained protein misfolding  
97 stress, we acutely depleted DR5 mRNA by siRNA prior to overexpressing MPZ-GFP.  
98 Knockdown of DR5 significantly reduced PARP cleavage and annexin V staining following  
99 overexpression of MPZ-GFP (Fig 1C-1D), which was not observed in control experiments  
100 expressing cytosolic GFP. To determine if upregulation of DR5 was sufficient to induce  
101 apoptosis, we increased DR5 levels in the absence of ER stress through ectopic expression of  
102 CHOP. Comparable levels of CHOP-induced DR5 protein in the absence of ER stress drove  
103 drastically lower levels of PARP cleavage and trypan blue staining (demarking apoptotic cells)  
104 compared to the presence of misfolded-protein stress (Fig 1–figure supplement 2A, 2C-2D).

105 These results show that DR5 activation does not occur spontaneously after its upregulation but  
106 requires additional input signals conveyed by ER stress.

107 To assess the molecular composition of activated DR5 assemblies formed in response  
108 to ER stress, we measured caspase 8 activity in cell extracts fractionated through size exclusion  
109 chromatography. We detected increased caspase 8 activity in high-molecular weight (MW)  
110 fractions of cells transfected with MPZ-GFP relative to GFP (Fig 1E). The fractions contained  
111 DR5 complexes and co-eluted with full-length MPZ-GFP but not GFP-degradation products (Fig.  
112 1E, lanes 2 and 4). Pull-down of DR5 from cell lysates enriched for FADD and MPZ-GFP (Fig  
113 1–figure supplement 3A), suggesting that the co-elution of DR5 and MPZ-GFP in the high MW  
114 fractions resulted from their physical association. To test if MPZ physically interacted with  
115 activated DR5 complexes, we immunoprecipitated MPZ-GFP and detected DR5, FADD, and  
116 caspase 8 (both full-length p55 and its cleaved form p43) (Fig 1F, Fig 1–figure supplement 3B).  
117 Furthermore, MPZ-GFP immunoprecipitates contained 2-3-fold more caspase 8 activity  
118 compared to empty beads (Fig 1G, Fig 1–figure supplement 3C), indicating that they contained  
119 assembled DISC in a similar degree as seen after affinity purification of TRAIL-ligated DR5  
120 (Hughes *et al.* 2013). In contrast, pull-down of cytosolic GFP did not enrich for DR5, FADD, or  
121 caspase activity (Fig 1F-1G), confirming the selectivity for ER-folded MPZ-GFP.

122 To determine if misfolded proteins generally induced caspase activity through  
123 association with DR5, we overexpressed GFP-tagged forms of two other ER-trafficked proteins,  
124 rhodopsin (RHO) and proinsulin (INS), which are also associated with CHOP-dependent cell  
125 death pathologies (W.-C. Chiang *et al.* 2016; Oyadomari *et al.* 2002). Sustained overexpression  
126 of both RHO-GFP and INS-GFP upregulated BiP and CHOP mRNAs (Fig 1–figure supplement  
127 4A) and induced *XBP1* mRNA splicing (Fig 1–figure supplement 4B). Both proteins formed  
128 SDS-insoluble aggregates and induced PARP cleavage and annexin V staining in a DR5-  
129 dependent manner (Fig 1–figure supplement 4C-4E). By contrast, immunoprecipitation of RHO-  
130 GFP enriched for DR5 protein and caspase 8 activity more robustly than INS-GFP (Fig 1–figure

131 supplement 5), despite inducing DR5-dependent apoptosis to a similar extent. This indicates  
132 that misfolded proteins differ in their propensity to directly engage the DR5-assembled DISC,  
133 and that other misfolded substrates—caused by the ectopically overexpressed ER-trafficked  
134 protein—may mediate direct DR5 activation. Thus, as exemplified by MPZ and RHO, a selective  
135 subset of misfolded proteins in the secretory pathway can engage DR5 to form oligomeric  
136 complexes that induce caspase 8 activation.

137

138 *Misfolded protein engages DR5 at the ER-Golgi intermediate compartment, inducing active DR5*  
139 *signaling clusters.*

140 To explore where within in the cell DR5 associated with misfolded protein, we used  
141 confocal imaging of fixed cells for immunofluorescence. These analyses revealed that  
142 intracellular MPZ-GFP and DR5 appeared in discrete puncta that often overlapped (Fig 2A).  
143 DR5 siRNA knockdown eliminated the DR5 signal, confirming the specificity of the DR5  
144 antibody (Fig 2—figure supplement 1A, right panel). Similarly, overexpression of RHO also  
145 resulted in intracellular puncta that frequently co-localized with DR5 clusters (Fig 2—figure  
146 supplement 1B). Quantification of the mean Pearson's correlation per cell demonstrated  
147 statistically significant overlap with DR5 signal for both GFP-tagged MPZ and RHO (Fig 2—figure  
148 supplement 1C), indicating that these misfolded proteins accumulate in the same compartment  
149 as DR5.

150 Previous findings suggested that DR5 is retained near the Golgi apparatus during ER  
151 stress (Lu *et al.* 2014). We confirmed co-localization with the purported Golgi marker RCAS1, as  
152 previously reported (Fig 2— figure supplement 1D). However, we observed little overlap in DR5  
153 staining with another *cis*-Golgi marker, giantin (Fig 2E). To resolve this discrepancy, we  
154 employed subcellular fractionation as an orthogonal biochemical approach. Separating  
155 organelle membranes revealed that RCAS1, DR5, and MPZ-GFP co-sedimented in fractions  
156 containing ERGIC53, a marker of the ER-Golgi intermediate compartment (ERGIC), but not with

157 those containing giantin (Fig 2B). Notably, a portion of FADD, a cytosolic protein expected to  
158 exclusively remain in the topmost, cytosolic fraction, migrated into the second fraction of the  
159 gradient, indicating its association with the ERGIC membranes. Consistent with the presence of  
160 FADD, the first and second ERGIC-associated fractions harbored the majority of the caspase 8  
161 activity in the cell lysate (Fig 2C), indicating the presence of active DR5 DISCs. Moreover,  
162 immunofluorescence with quantification of the mean correlation per cell demonstrated the co-  
163 localization of DR5 with the ERGIC rather than with the Golgi (Fig 2D, 2F).

164 To determine when DR5 accumulates at the ERGIC relative to misfolded proteins, we  
165 compared the immunofluorescence of cells fixed at 20 hours (before the onset of caspase  
166 activity) and at 24 hours post-transfection (after the onset of caspase activity, Fig 1–figure  
167 supplement 1E). Intracellular puncta of MPZ appeared at 20 hours, preceding the appearance  
168 of DR5 clusters at 24 hours (Fig 2–figure supplement 2A). Between 20 and 24 hours, the  
169 correlation of DR5 and ERGIC53 increased, whereas the correlation of MPZ with ERGIC53  
170 remained steady, indicating that DR5 accumulated after saturation of MPZ levels at the ERGIC  
171 (Fig 2–figure supplement 2B-2C). By contrast, the mean Pearson’s correlation with giantin  
172 approached zero for both MPZ and DR5 at 24 hours post-transfection (Fig 2–figure supplement  
173 2B, Fig 2F). These results confirm the localization of DR5 and misfolded protein at the ERGIC  
174 under conditions of unmitigated ER stress.

175

176 *Polypeptide sequences of mammalian ER-trafficked protein directly bind to the DR5 ectodomain*  
177 *and induce its oligomerization..*

178 With evidence of a physical association between misfolded protein and active DR5  
179 oligomers at the ERGIC, we asked how misfolded proteins and DR5 interact. Considering the  
180 precedence that i) DR5 binds unstructured peptides mimicking TRAIL (Kajiwara *et al.* 2004;  
181 Pavet *et al.* 2010) and ii) that UPR sensors can directly bind misfolded protein to sense ER  
182 stress (Karagöz *et al.* 2017; Wang *et al.* 2018; Gardner and Walter 2011), we hypothesized that

183 DR5 may directly recognize unstructured regions of misfolded proteins through its ectodomain  
184 (ECD) that would project into the ERGIC lumen. Probing a peptide array with purified  
185 recombinant Fc-tagged DR5 ECD revealed promiscuous recognition of amino acid sequences  
186 throughout the ectodomain of MPZ and within extracellular loops of RHO (Fig 3A, Fig 3–figure  
187 supplement 1A-1B). Quantification of the relative signal intensity revealed that DR5-binding  
188 sequences were enriched for aliphatic and aromatic residues whereas polar and acidic residues  
189 were excluded (Fig 3–figure supplement 1C), reminiscent of qualities that become surface-  
190 exposed in misfolded or unfolded proteins.

191 To validate the specificity of DR5 interactions on the array, we performed pull-down  
192 assays on the MPZ-derived peptide exhibiting the strongest signal (spots C18-C19 in Fig 3A,  
193 hereon referred to as MPZ-ecto) with recombinant Fc-tagged DR5 ECD versus TNFR1 ECD as  
194 a selectivity control. The MPZ-ecto peptide bound specifically to the DR5 ECD but not the  
195 TNFR1 ECD (Fig 3B). Under equilibrium conditions, interaction with MPZ-ecto peptide  
196 quenched fluorescently labeled DR5 ECD but not fluorescently labeled TNFR1 ECD, yielding an  
197 apparent binding affinity of  $K_{1/2} = 109 \mu\text{M} \pm 11 \mu\text{M}$  with a Hill coefficient of 2.6 (Fig 3C, Fig 3–  
198 figure supplement 2A). Adding excess unlabeled DR5 ECD restored fluorescence (Fig 3–figure  
199 supplement 2B), indicating that the quenching reflected a specific and reversible interaction  
200 between the DR5 ECD and the MPZ-ecto peptide. Moreover, mutation of two aromatic amino  
201 acids (both Tyr) to disfavored acidic amino acids (Glu) abrogated binding (Fig 3C),  
202 demonstrating that the interaction is sequence-specific.

203 The Hill coefficient of 2.6 suggested cooperative binding. Therefore, we tested if the DR5  
204 ECD forms oligomers in the presence of peptide. In the absence of peptide, the addition of a  
205 chemical cross-linker captured dimers of FLAG-tagged DR5 ECD (Fig 3D, Fig 3–figure  
206 supplement 2C), consistent with pre-ligand assembled dimers previously observed for members  
207 of the TNFR family (Clancy *et al.* 2005; Siegel *et al.* 2000; Chan *et al.* 2000) . With increasing  
208 concentration of peptide (up to 200  $\mu\text{M}$ ), crosslinking revealed multimers of the DR5 ECD (Fig



209 3D), indicating that the peptide acts as a ligand to template assembly of DR5 oligomers.  
210 Interestingly, excess peptide (400  $\mu$ M) dissociated higher-order oligomers of DR5, suggesting a  
211 lower valency of interaction when the DR5 concentration becomes limiting.

212 To examine the DR5 oligomerization at saturating peptide concentrations by an  
213 orthogonal method, we fractionated DR5 ECD-peptide complexes using size exclusion  
214 chromatography. At 100  $\mu$ M MPZ-ecto ( $\sim K_{1/2}$ ), DR5 ECD co-eluted with the peptide as higher-  
215 order oligomers near the void volume (7-8 ml) and as apo-dimers centered at 14 ml, as shown  
216 in the Coomassie blue-stained gel for DR5 and fluorescence scan for fluorescein-labeled MPZ-  
217 ecto peptide (Fig 3E-3F, green outline). This elution pattern was similar to that of the DR5 ECD-  
218 TRAIL complex, for which both proteins co-eluted near the void volume (Fig 3-figure  
219 supplement 2E-2F). However, with excess MPZ-ecto peptide at 400  $\mu$ M (4-times  $K_{1/2}$ ), the  
220 proportion of higher-order oligomers of DR5 ECD and the peptide diminished and re-distributed  
221 to later eluting fractions at 12-15 ml (Fig 3-figure supplement 2G-2H, teal outline), indicating  
222 disassembly into smaller oligomers of DR5 ECD and pointing at the reversibility of the higher-  
223 order DR5-peptide assemblies. Importantly, the non-binding peptide bearing the Tyr-to-Glu  
224 substitutions did not co-migrate with or induce the oligomerization of DR5 ECD (Fig 3E-3F,  
225 magenta outline).

226

227 *Disrupting misfolded protein binding to DR5 attenuates ER stress-mediated apoptosis.*

228 Since mutating the Tyr residues to Glu on the MPZ-ecto peptide proved sufficient to  
229 disrupt the DR5 ECD interaction in solution, we tested the ability of this minimal MPZ-derived  
230 sequence to bind to and activate DR5 in cells. To this end, we generated constructs that  
231 replaced the ectodomain of MPZ with either the MPZ-ecto peptide, the peptide sequence with  
232 Tyr-to-Glu substitutions, or the peptide with all its aromatic residues changed to Glu to further  
233 deplete DR5-favored amino acid side chains revealed in the peptide array (Fig 4A). In a titration  
234 of MPZ-ecto peptide expression, the WT peptide sequence induced more PARP cleavage and

235 caspase activity than similar or higher levels of the peptides containing Glu substitutions (Fig  
236 4B, compare lanes 5, 7, and 10, Fig 4C). The Glu-containing peptides also induced reduced  
237 PARP cleavage in another epithelial cell type, HepG2 (Fig 4– figure supplement 1A). Acute  
238 knockdown of DR5 reduced PARP cleavage during MPZ-ecto peptide expression, while  
239 exogenous FLAG-tagged DR5 expression restored PARP cleavage (Fig 4–figure supplement  
240 1B). Of note, depletion of DR5 resulted in detection of higher levels of the MPZ-ecto peptide,  
241 likely because cells with this protein-folding burden were not eliminated.

242         Expressing comparable levels of the MPZ-ecto peptide and its variants (using conditions  
243 of lanes 5, 7, and 10 in Fig 4B) induced *XBP1* mRNA splicing and transcription of CHOP and  
244 BiP mRNAs, indicating that the presence of these peptides perturb ER protein folding  
245 homeostasis to a similar degree (Fig 4D, Fig 4E). Immunofluorescence showed that the MPZ-  
246 ecto peptide localized to the plasma membrane and within intracellular puncta that partially  
247 overlapped with ERGIC signal, although to a lesser extent than overexpressed full-length MPZ  
248 (Fig 4F, Fig 4–figure supplement 2C). The Glu-containing mutant peptides were similarly  
249 distributed within cells with no significant difference in their average correlation with ERGIC  
250 signal (Fig 4–figure supplement 2A-2B). DR5, in all three conditions, also showed a positive  
251 correlation with the ERGIC marker (Fig 4–figure supplement 2E). To determine if DR5  
252 interacted with the MPZ-ecto peptide or its mutants, we immunoprecipitated the GFP-tagged  
253 peptides. Pulldown of the MPZ-ecto peptide enriched for DR5 relative to the Glu-containing  
254 mutant peptides (Fig 4G, Fig 4–figure supplement 3A). Consistent with this specific enrichment  
255 of DR5 for the WT sequence, PARP cleavage and caspase activity measured in cell lysates  
256 were increased with the WT MPZ-ecto relative to the mutants (Fig 4B-4C). To confirm that the  
257 expression of MPZ-ecto peptide induces apoptotic cell death, we measured annexin V staining  
258 in the absence and presence of the pan-caspase inhibitor z-VAD (Fig 4H, Figure 4–figure  
259 supplement 2C-2D). As expected, expressing the MPZ-ecto peptide increased annexin V  
260 staining relative to the empty vector but treatment with zVAD diminished the extent of annexin

261 V staining (Fig 4H). Importantly, cells expressing the Glu-containing mutant peptides exhibit  
262 decreased annexin V staining, demonstrating that DR5 binding of exposed polypeptides on  
263 misfolded protein is important for driving apoptosis.

264

## 265 **Discussion**

266 Our data identify misfolded protein as the ER stress factor that switches upregulated  
267 DR5 from its inactive auto-inhibited dimer state to active multimeric clusters to initiate DISC  
268 assembly and apoptosis at the ER-Golgi intermediate complex. We have examined the  
269 mechanism of apoptosis induction by the sustained expression of three different candidate ER-  
270 trafficked proteins associated with CHOP-dependent disease pathologies: MPZ, RHO, and INS  
271 (Pennuto *et al.* 2008; W. C. Chiang *et al.* 2016; Oyadomari *et al.* 2002). In epithelial cells,  
272 overexpression of each protein induces apoptosis in a DR5-dependent manner. Consistent with  
273 previous reports of ectopic CHOP expression in the absence of ER stress (McCullough *et al.*  
274 2001; Han *et al.* 2013; Southwood *et al.* 2016), CHOP-driven upregulation of DR5 alone did not  
275 account for the apoptosis observed during the overexpression of an ER-trafficked protein. For  
276 MPZ and RHO, the intracellular, misfolded pools of each protein physically associated with the  
277 DR5-caspase 8 complex. For proinsulin, which weakly associated with DR5 but triggered  
278 apoptosis to a similar extent, we believe it is likely that overexpression of this singular protein  
279 perturbed the folding of endogenous trafficking substrates and thereby provided other, perhaps  
280 more favored, misfolding substrates to directly engage DR5. This latter scenario is likely to  
281 occur under pharmacologically induced ER stress as well. The interaction between misfolded  
282 protein and DR5 bridges the long-standing mechanistic gap of why CHOP expression (and  
283 subsequent upregulation of its downstream factors) is necessary but not sufficient to drive cell  
284 death. Through characterizing the interaction between the DR5 ECD and peptide sequences of  
285 ER-trafficked proteins, we demonstrate that DR5 promiscuously binds to exposed hydrophobic

286 stretches of misfolded proteins with an affinity in the range of 100  $\mu$ M and in a highly  
287 cooperative manner.

288         To grasp how such a high concentration of misfolded protein could occur in the ERGIC,  
289 it is important to consider that the compartment is composed of vesicles and tubules measuring  
290 60-100 nm in diameter and <500 nm in length. In a back-of-the-envelope calculation, we  
291 estimate that reaching 100  $\mu$ M in a vesicle with a diameter of 100 nm would require only 32  
292 molecules (Sesso *et al.* 1994; Fan, Roth, and Zuber 2003). The measured affinities are  
293 therefore well within physiological range. Quantitative fluorescence microscopy of living COS7  
294 cells has indicated up to 100 molecules of a GFP-tagged viral glycoprotein in a 100-nm vesicle  
295 (Hirschberg *et al.* 1998), providing experimental evidence that surpassing concentrations of 100  
296  $\mu$ M is indeed physiologically relevant. In fact, the “low” affinity between DR5 and misfolded  
297 proteins is likely a necessary feature that prevents aberrant DR5 oligomerization and activation  
298 in the crowded luminal environment of membrane-bound compartments, as we previously  
299 established for other unfolded protein sensors, such as IRE1 (Gardner *et al.* 2013; Gardner and  
300 Walter 2011; Karagöz *et al.* 2017).

301         Given that misfolded receptors can be exported from the ER when quality control  
302 mechanisms are overwhelmed (Satpute-Krishnan *et al.* 2014; Sirkis, Aparicio, and Schekman  
303 2017), detection of misfolded proteins by DR5 downstream of the ER likely serves to prevent  
304 the cell from displaying or secreting dysfunctional proteins that would be detrimental in a  
305 multicellular context. While IRE1 and PERK act as initial UPR sensors in the ER, DR5 acts as a  
306 late sensor of misfolded protein at the ERGIC during unmitigated ER stress. Thus, intracellular  
307 DR5 triggers apoptosis to enforce a terminal quality control checkpoint for secretory and  
308 transmembrane proteins. We postulate that other members of the TNFR family, e.g. DR4, which  
309 has been reported to play a role in cell death during Golgi stress (van Raam *et al.* 2017), may  
310 respond similarly to intracellular stimuli.

311         Although extensive research has focused on the therapeutic activation of death

312 receptors including DR5 (Avi Ashkenazi 2015), limited strategies exist to inhibit such receptors  
313 despite their demonstrated role in apoptosis-mediated disease progression (Vunnam et al.  
314 2017). Namely, DR5-mediated apoptosis in hepatocytes has been linked to non-alcoholic fatty  
315 liver disease, while CHOP-dependent apoptosis in Schwann cells—wherein a role for DR5 has  
316 yet to be investigated—may contribute to diabetic peripheral neuropathies (Cazanave et al.  
317 2011; Sato et al. 2015). Our finding that the assembly and disassembly of DR5 ECD oligomers  
318 can be controlled by a peptide raises the possibility that intracellular DR5 activation could be  
319 inhibited through small molecule ligand-induced dissociation of DR5 clusters to prevent  
320 apoptosis and thus preserve cell viability in the face of unresolved ER stress. From the work  
321 herein, this notion now emerges as a promising strategy to interfere therapeutically with  
322 deleterious death receptor function.

323

324 **References**

- 325 Ashkenazi, A, and V M Dixit. 1998. "Death Receptors: Signaling and Modulation." *Science (New*  
326 *York, N. Y.)* 281 (5381). American Association for the Advancement of Science: 1305–8.  
327 <https://doi.org/10.1126/SCIENCE.281.5381.1305>.
- 328 Ashkenazi, Avi. 2015. "Targeting the Extrinsic Apoptotic Pathway in Cancer: Lessons Learned  
329 and Future Directions." *The Journal of Clinical Investigation* 125 (2). American Society for  
330 Clinical Investigation: 487–89. <https://doi.org/10.1172/JCI80420>.
- 331 Carpenter, Anne E, Thouis R Jones, Michael R Lamprecht, Colin Clarke, In Kang, Ola Friman,  
332 David A Guertin, et al. 2006. "CellProfiler: Image Analysis Software for Identifying and  
333 Quantifying Cell Phenotypes." *Genome Biology* 7 (10): R100. [https://doi.org/10.1186/gb-](https://doi.org/10.1186/gb-2006-7-10-r100)  
334 [2006-7-10-r100](https://doi.org/10.1186/gb-2006-7-10-r100).
- 335 Cazanave, Sophie C, Justin L Mott, Steven F Bronk, Nathan W Werneburg, Christian D Fingas,  
336 X Wei Meng, Niklas Finnberg, Wafik S El-Deiry, Scott H Kaufmann, and Gregory J Gores.  
337 2011. "Death Receptor 5 Signaling Promotes Hepatocyte Lipoapoptosis." *The Journal of*  
338 *Biological Chemistry* 286 (45). American Society for Biochemistry and Molecular Biology:  
339 39336–48. <https://doi.org/10.1074/jbc.M111.280420>.
- 340 Chan, F K, H J Chun, L Zheng, R M Siegel, K L Bui, and M J Lenardo. 2000. "A Domain in TNF  
341 Receptors That Mediates Ligand-Independent Receptor Assembly and Signaling." *Science*  
342 *(New York, N. Y.)* 288 (5475): 2351–54. <http://www.ncbi.nlm.nih.gov/pubmed/10875917>.
- 343 Chang, Tsun-Kai, David A. Lawrence, Min Lu, Jenille Tan, Jonathan M. Harnoss, Scot A.  
344 Marsters, Peter Liu, Wendy Sandoval, Scott E. Martin, and Avi Ashkenazi. 2018.  
345 "Coordination between Two Branches of the Unfolded Protein Response Determines  
346 Apoptotic Cell Fate." *Molecular Cell* 71 (4). Cell Press: 629–636.e5.  
347 <https://doi.org/10.1016/J.MOLCEL.2018.06.038>.
- 348 Chiang, Wei-Chieh, Victory Joseph, Douglas Yasumura, Michael T. Matthes, Alfred S. Lewin,  
349 Marina S. Gorbatyuk, Kelly Ahern, Matthew M. LaVail, and Jonathan H. Lin. 2016.

- 350 “Ablation of Chop Transiently Enhances Photoreceptor Survival but Does Not Prevent  
351 Retinal Degeneration in Transgenic Mice Expressing Human P23H Rhodopsin.” In  
352 *Advances in Experimental Medicine and Biology*, 854:185–91. [https://doi.org/10.1007/978-](https://doi.org/10.1007/978-3-319-17121-0_25)  
353 [3-319-17121-0\\_25](https://doi.org/10.1007/978-3-319-17121-0_25).
- 354 Chiang, Wei Chieh, Victory Joseph, Douglas Yasumura, Michael T. Matthes, Alfred S. Lewin,  
355 Marina S. Gorbatyuk, Kelly Ahern, Matthew M. Lavail, and Jonathan H. Lin. 2016. “Ablation  
356 of Chop Transiently Enhances Photoreceptor Survival but Does Not Prevent Retinal  
357 Degeneration in Transgenic Mice Expressing Human P23H Rhodopsin.” In *Advances in*  
358 *Experimental Medicine and Biology*, 854:185–91. Springer New York LLC.  
359 [https://doi.org/10.1007/978-3-319-17121-0\\_25](https://doi.org/10.1007/978-3-319-17121-0_25).
- 360 Clancy, Lauren, Karen Mruk, Kristina Archer, Melissa Woelfel, Juthathip Mongkolsapaya, Gavin  
361 Screaton, Michael J Lenardo, and Francis Ka-Ming Chan. 2005. “Preligand Assembly  
362 Domain-Mediated Ligand-Independent Association between TRAIL Receptor 4 (TR4) and  
363 TR2 Regulates TRAIL-Induced Apoptosis.” *Proceedings of the National Academy of*  
364 *Sciences of the United States of America* 102 (50): 18099–104.  
365 <https://doi.org/10.1073/pnas.0507329102>.
- 366 Dickens, Laura S., Robert S. Boyd, Rebekah Jukes-Jones, Michelle A. Hughes, Gemma L.  
367 Robinson, Louise Fairall, John W.R. Schwabe, Kelvin Cain, and Marion MacFarlane. 2012.  
368 “A Death Effector Domain Chain DISC Model Reveals a Crucial Role for Caspase-8 Chain  
369 Assembly in Mediating Apoptotic Cell Death.” *Molecular Cell* 47 (2). Cell Press: 291–305.  
370 <https://doi.org/10.1016/J.MOLCEL.2012.05.004>.
- 371 Dufour, Florent, Thibault Rattier, Andrei Alexandru Constantinescu, Luciana Zischler, Aymeric  
372 Morlé, Hazem Ben Mabrouk, Etienne Humblin, et al. 2017. “TRAIL Receptor Gene Editing  
373 Unveils TRAIL-R1 as a Master Player of Apoptosis Induced by TRAIL and ER Stress.”  
374 *Oncotarget* 8 (6): 9974–85. <https://doi.org/10.18632/oncotarget.14285>.
- 375 Fan, Jing-Yu, Jürgen Roth, and Christian Zuber. 2003. “Ultrastructural Analysis of Transitional

- 376 Endoplasmic Reticulum and Pre-Golgi Intermediates: A Highway for Cars and Trucks.”  
377 *Histochemistry and Cell Biology* 120 (6). Springer-Verlag: 455–63.  
378 <https://doi.org/10.1007/s00418-003-0597-1>.
- 379 Gardner, B. M., D. Pincus, K. Gotthardt, C. M. Gallagher, and P. Walter. 2013. “Endoplasmic  
380 Reticulum Stress Sensing in the Unfolded Protein Response.” *Cold Spring Harbor*  
381 *Perspectives in Biology* 5 (3): a013169–a013169.  
382 <https://doi.org/10.1101/cshperspect.a013169>.
- 383 Gardner, B. M., and P. Walter. 2011. “Unfolded Proteins Are Ire1-Activating Ligands That  
384 Directly Induce the Unfolded Protein Response.” *Science* 333 (6051): 1891–94.  
385 <https://doi.org/10.1126/science.1209126>.
- 386 Han, Jaeseok, Sung Hoon Back, Junguk Hur, Yu-Hsuan Lin, Robert Gildersleeve, Jixiu Shan,  
387 Celvie L. Yuan, et al. 2013. “ER-Stress-Induced Transcriptional Regulation Increases  
388 Protein Synthesis Leading to Cell Death.” *Nature Cell Biology* 15 (5). Nature Publishing  
389 Group: 481–90. <https://doi.org/10.1038/ncb2738>.
- 390 Harding, Heather P, Yuhong Zhang, Huiquing Zeng, Isabel Novoa, Phoebe D Lu, Marcella  
391 Calfon, Navid Sadri, et al. 2003. “An Integrated Stress Response Regulates Amino Acid  
392 Metabolism and Resistance to Oxidative Stress.” *Molecular Cell* 11 (3): 619–33.  
393 <http://www.ncbi.nlm.nih.gov/pubmed/12667446>.
- 394 Hirschberg, K, C M Miller, J Ellenberg, J F Presley, E D Siggia, R D Phair, and J Lippincott-  
395 Schwartz. 1998. “Kinetic Analysis of Secretory Protein Traffic and Characterization of Golgi  
396 to Plasma Membrane Transport Intermediates in Living Cells.” *The Journal of Cell Biology*  
397 143 (6). The Rockefeller University Press: 1485–1503.  
398 <https://doi.org/10.1083/jcb.143.6.1485>.
- 399 Hughes, Michelle A., Claudia Langlais, Kelvin Cain, and Marion MacFarlane. 2013. “Isolation,  
400 Characterisation and Reconstitution of Cell Death Signalling Complexes.” *Methods* 61 (2).  
401 Academic Press: 98–104. <https://doi.org/10.1016/J.YMETH.2013.02.006>.



- 402 Hymowitz, Sarah G., Hans W. Christinger, Germaine Fuh, Mark Ultsch, Mark O'Connell, Robert  
403 F. Kelley, Avi Ashkenazi, and Abraham M. De Vos. 1999. "Triggering Cell Death: The  
404 Crystal Structure of Apo2L/TRAIL in a Complex with Death Receptor 5." *Molecular Cell* 4  
405 (4). Cell Press: 563–71. [https://doi.org/10.1016/S1097-2765\(00\)80207-5](https://doi.org/10.1016/S1097-2765(00)80207-5).
- 406 Iurlaro, Raffaella, Franziska Püschel, Clara Lucía León-Annicchiarico, Hazel O'Connor, Seamus  
407 J Martin, Daniel Palou-Gramón, Estefanía Lucendo, and Cristina Muñoz-Pinedo. 2017.  
408 "Glucose Deprivation Induces ATF4-Mediated Apoptosis through TRAIL Death Receptors."  
409 *Molecular and Cellular Biology* 37 (10): e00479-16. <https://doi.org/10.1128/MCB.00479-16>.
- 410 Jin, Zhaoyu, Yun Li, Robert Pitti, David Lawrence, Victoria C. Pham, Jennie R. Lill, and Avi  
411 Ashkenazi. 2009. "Cullin3-Based Polyubiquitination and p62-Dependent Aggregation of  
412 Caspase-8 Mediate Extrinsic Apoptosis Signaling." *Cell* 137 (4). Cell Press: 721–35.  
413 <https://doi.org/10.1016/J.CELL.2009.03.015>.
- 414 Kajiwara, Kazumi, Atsuhiko Saito, Shin-ichi Ogata, and Masao Tanihara. 2004. "Synthetic  
415 Peptides Corresponding to Ligand-Binding Region of Death Receptors, DR5, Fas, and  
416 TNFR, Specifically Inhibit Cell Death Mediated by the Death Ligands, Respectively."  
417 *Biochimica et Biophysica Acta (BBA) - Proteins and Proteomics* 1699 (1–2): 131–37.  
418 <https://doi.org/10.1016/j.bbapap.2004.02.016>.
- 419 Karagöz, G Elif, Diego Acosta-Alvear, Hieu T Nguyen, Crystal P Lee, Feixia Chu, and Peter  
420 Walter. 2017. "An Unfolded Protein-Induced Conformational Switch Activates Mammalian  
421 IRE1." *eLife* 6 (October). eLife Sciences Publications, Ltd.  
422 <https://doi.org/10.7554/eLife.30700>.
- 423 Kischkel, F C, D A Lawrence, A Chuntharapai, P Schow, K J Kim, and A Ashkenazi. 2000.  
424 "Apo2L/TRAIL-Dependent Recruitment of Endogenous FADD and Caspase-8 to Death  
425 Receptors 4 and 5." *Immunity* 12 (6): 611–20.  
426 <http://www.ncbi.nlm.nih.gov/pubmed/10894161>.
- 427 Lam, Mable, David A Lawrence, Avi Ashkenazi, and Peter Walter. 2018. "Confirming a Critical

- 428 Role for Death Receptor 5 and Caspase-8 in Apoptosis Induction by Endoplasmic  
429 Reticulum Stress.” *Cell Death and Differentiation* 25 (8): 1530–31.  
430 <https://doi.org/10.1038/s41418-018-0155-y>.
- 431 LeBlanc, Heidi, David Lawrence, Eugene Varfolomeev, Klara Totpal, John Morlan, Peter  
432 Schow, Sharon Fong, Ralph Schwall, Dominick Sinicropi, and Avi Ashkenazi. 2002.  
433 “Tumor-Cell Resistance to Death Receptor–induced Apoptosis through Mutational  
434 Inactivation of the Proapoptotic Bcl-2 Homolog Bax.” *Nature Medicine* 8 (3). Nature  
435 Publishing Group: 274–81. <https://doi.org/10.1038/nm0302-274>.
- 436 Lu, M., D. A. Lawrence, S. Marsters, D. Acosta-Alvear, P. Kimmig, A. S. Mendez, A. W. Paton,  
437 J. C. Paton, P. Walter, and A. Ashkenazi. 2014. “Opposing Unfolded-Protein-Response  
438 Signals Converge on Death Receptor 5 to Control Apoptosis.” *Science* 345 (6192): 98–  
439 101. <https://doi.org/10.1126/science.1254312>.
- 440 McCullough, K D, J L Martindale, L O Klotz, T Y Aw, and N J Holbrook. 2001. “Gadd153  
441 Sensitizes Cells to Endoplasmic Reticulum Stress by down-Regulating Bcl2 and Perturbing  
442 the Cellular Redox State.” *Molecular and Cellular Biology* 21 (4): 1249–59.  
443 <https://doi.org/10.1128/MCB.21.4.1249-1259.2001>.
- 444 Mongkolsapaya, Juthathip, Jonathan M. Grimes, Nan Chen, Xiao Ning Xu, David I. Stuart, E.  
445 Yvonne Jones, and Gavin R. Screaton. 1999. “Structure of the TRAIL-DR5 Complex  
446 Reveals Mechanisms Conferring Specificity in Apoptotic Initiation.” *Nature Structural  
447 Biology* 6 (11): 1048–53. <https://doi.org/10.1038/14935>.
- 448 Muzio, Marta, Brent R. Stockwell, Henning R. Stennicke, Guy S. Salvesen, and Vishva M. Dixit.  
449 1998. “An Induced Proximity Model for Caspase-8 Activation.” *Journal of Biological  
450 Chemistry* 273 (5): 2926–30. <https://doi.org/10.1074/jbc.273.5.2926>.
- 451 Oyadomari, Seiichi, Akio Koizumi, Kiyoshi Takeda, Tomomi Gotoh, Shizuo Akira, Eiichi Araki,  
452 and Masataka Mori. 2002. “Targeted Disruption of the Chop Gene Delays Endoplasmic  
453 Reticulum Stress–mediated Diabetes.” *Journal of Clinical Investigation* 109 (4): 525–32.

- 454 <https://doi.org/10.1172/JCI14550>.
- 455 Pan, Liqiang, Tian-Min Fu, Wenbin Zhao, Linlin Zhao, Wen Chen, Chixiao Qiu, Wenhui Liu, et  
456 al. 2019. "Higher-Order Clustering of the Transmembrane Anchor of DR5 Drives  
457 Signaling." *Cell* 0 (0). Elsevier. <https://doi.org/10.1016/j.cell.2019.02.001>.
- 458 Pavet, V., J. Beyrath, C. Pardin, A. Morizot, M.-C. Lechner, J.-P. Briand, M. Wendland, et al.  
459 2010. "Multivalent DR5 Peptides Activate the TRAIL Death Pathway and Exert Tumoricidal  
460 Activity." *Cancer Research* 70 (3): 1101–10. [https://doi.org/10.1158/0008-5472.CAN-09-](https://doi.org/10.1158/0008-5472.CAN-09-2889)  
461 2889.
- 462 Pennuto, Maria, Elisa Tinelli, MariaChiara Malaguti, Ubaldo Del Carro, Maurizio D'Antonio,  
463 David Ron, Angelo Quattrini, M. Laura Feltri, and Lawrence Wrabetz. 2008. "Ablation of the  
464 UPR-Mediator CHOP Restores Motor Function and Reduces Demyelination in Charcot-  
465 Marie-Tooth 1B Mice." *Neuron* 57 (3). Cell Press: 393–405.  
466 <https://doi.org/10.1016/J.NEURON.2007.12.021>.
- 467 Pitti, Robert M., Scot A. Marsters, Siegfried Ruppert, Christopher J. Donahue, Alison Moore,  
468 and Avi Ashkenazi. 1996. "Induction of Apoptosis by Apo-2 Ligand, a New Member of the  
469 Tumor Necrosis Factor Cytokine Family." *Journal of Biological Chemistry* 271 (22): 12687–  
470 90. <https://doi.org/10.1074/jbc.271.22.12687>.
- 471 Raam, Bram J van, Tamara Lacina, Ralph K Lindemann, and Jan H Reiling. 2017. "Secretory  
472 Stressors Induce Intracellular Death Receptor Accumulation to Control Apoptosis." *Cell*  
473 *Death & Disease* 8 (10): e3069. <https://doi.org/10.1038/cddis.2017.466>.
- 474 Sato, Keisuke, Ryosuke Tatsunami, Kaori Yama, Yu Murao, and Yoshiko Tampo. 2015.  
475 "Glycolaldehyde Induces Endoplasmic Reticulum Stress and Apoptosis in Schwann Cells."  
476 *Toxicology Reports* 2 (January). Elsevier: 1454–62.  
477 <https://doi.org/10.1016/J.TOXREP.2015.10.014>.
- 478 Satpute-Krishnan, Prasanna, Monica Ajinkya, Savithri Bhat, Eisuke Itakura, Ramanujan S.  
479 Hegde, and Jennifer Lippincott-Schwartz. 2014. "ER Stress-Induced Clearance of

- 480 Misfolded GPI-Anchored Proteins via the Secretory Pathway.” *Cell* 158 (3): 522–33.  
481 <https://doi.org/10.1016/j.cell.2014.06.026>.
- 482 Sesso, A, F P de Faria, E S Iwamura, and H Corrêa. 1994. “A Three-Dimensional  
483 Reconstruction Study of the Rough ER-Golgi Interface in Serial Thin Sections of the  
484 Pancreatic Acinar Cell of the Rat.” *Journal of Cell Science* 107 ( Pt 3) (March): 517–28.  
485 <http://www.ncbi.nlm.nih.gov/pubmed/8006070>.
- 486 Sheridan, J P, S A Marsters, R M Pitti, A Gurney, M Skubatch, D Baldwin, L Ramakrishnan, et  
487 al. 1997. “Control of TRAIL-Induced Apoptosis by a Family of Signaling and Decoy  
488 Receptors.” *Science (New York, N. Y.)* 277 (5327): 818–21.  
489 <http://www.ncbi.nlm.nih.gov/pubmed/9242611>.
- 490 Siegel, R M, J K Frederiksen, D A Zacharias, F K Chan, M Johnson, D Lynch, R Y Tsien, and M  
491 J Lenardo. 2000. “Fas Preassociation Required for Apoptosis Signaling and Dominant  
492 Inhibition by Pathogenic Mutations.” *Science (New York, N. Y.)* 288 (5475): 2354–57.  
493 <http://www.ncbi.nlm.nih.gov/pubmed/10875918>.
- 494 Sirkis, Daniel W, Renan E Aparicio, and Randy Schekman. 2017. “Neurodegeneration-  
495 Associated Mutant TREM2 Proteins Abortively Cycle between the ER and ER-Golgi  
496 Intermediate Compartment.” *Molecular Biology of the Cell* 28 (20): 2723–33.  
497 <https://doi.org/10.1091/mbc.E17-06-0423>.
- 498 Southwood, Cherie M., Bozena Fykolodziej, Kathleen J. Maheras, Danielle M. Garshott, Molly  
499 Estill, Andrew M. Fribley, and Alexander Gow. 2016. “Overexpression of CHOP in  
500 Myelinating Cells Does Not Confer a Significant Phenotype under Normal or Metabolic  
501 Stress Conditions.” *The Journal of Neuroscience* 36 (25): 6803–19.  
502 <https://doi.org/10.1523/JNEUROSCI.1118-15.2016>.
- 503 Spierings, Diana C., Elisabeth G. de Vries, Edo Vellenga, Fiona A. van den Heuvel, Jan J.  
504 Koornstra, Jelle Wesseling, Harry Hollema, and Steven de Jong. 2004. “Tissue Distribution  
505 of the Death Ligand TRAIL and Its Receptors.” *Journal of Histochemistry & Cytochemistry*

- 506 52 (6): 821–31. <https://doi.org/10.1369/jhc.3A6112.2004>.
- 507 Sprick, M R, M A Weigand, E Rieser, C T Rauch, P Juo, J Blenis, P H Krammer, and H  
508 Walczak. 2000. “FADD/MORT1 and Caspase-8 Are Recruited to TRAIL Receptors 1 and 2  
509 and Are Essential for Apoptosis Mediated by TRAIL Receptor 2.” *Immunity* 12 (6): 599–  
510 609. <http://www.ncbi.nlm.nih.gov/pubmed/10894160>.
- 511 Tabas, Ira, and David Ron. 2011. “Integrating the Mechanisms of Apoptosis Induced by  
512 Endoplasmic Reticulum Stress.” *Nature Cell Biology* 13 (3): 184–90.  
513 <https://doi.org/10.1038/ncb0311-184>.
- 514 Valley, Christopher C., Andrew K. Lewis, Deepti J. Mudaliar, Jason D. Perlmutter, Anthony R.  
515 Braun, Christine B. Karim, David D. Thomas, Jonathan R. Brody, and Jonathan N. Sachs.  
516 2012. “Tumor Necrosis Factor-Related Apoptosis-Inducing Ligand (TRAIL) Induces Death  
517 Receptor 5 Networks That Are Highly Organized.” *Journal of Biological Chemistry* 287 (25):  
518 21265–78. <https://doi.org/10.1074/jbc.M111.306480>.
- 519 Vanamee, Éva S, and Denise L Faustman. 2018. “Structural Principles of Tumor Necrosis  
520 Factor Superfamily Signaling.” *Science Signaling* 11 (511). American Association for the  
521 Advancement of Science: eaao4910. <https://doi.org/10.1126/scisignal.aao4910>.
- 522 Vunnam, Nagamani, Chih Hung Lo, Benjamin D. Grant, David D. Thomas, and Jonathan N.  
523 Sachs. 2017. “Soluble Extracellular Domain of Death Receptor 5 Inhibits TRAIL-Induced  
524 Apoptosis by Disrupting Receptor–Receptor Interactions.” *Journal of Molecular Biology* 429  
525 (19). Academic Press: 2943–53. <https://doi.org/10.1016/J.JMB.2017.08.009>.
- 526 Walczak, H., M A Degli-Esposti, R S Johnson, P J Smolak, J Y Waugh, N Boiani, M S Timour,  
527 et al. 1997. “TRAIL-R2: A Novel Apoptosis-Mediating Receptor for TRAIL.” *The EMBO*  
528 *Journal* 16 (17): 5386–97. <https://doi.org/10.1093/emboj/16.17.5386>.
- 529 Walter, P., and D. Ron. 2011. “The Unfolded Protein Response: From Stress Pathway to  
530 Homeostatic Regulation.” *Science* 334 (6059): 1081–86.  
531 <https://doi.org/10.1126/science.1209038>.

- 532 Wang, Peng, Jingzhi Li, Jiahui Tao, and Bingdong Sha. 2018. "The Luminal Domain of the ER  
533 Stress Sensor Protein PERK Binds Misfolded Proteins and Thereby Triggers PERK  
534 Oligomerization." *Journal of Biological Chemistry* 293 (11): 4110–21.  
535 <https://doi.org/10.1074/jbc.RA117.001294>.
- 536 Wei, M. C., W. X. Zong, E. H.Y. Cheng, T. Lindsten, V. Panoutsakopoulou, A. J. Ross, K. A.  
537 Roth, G. R. Macgregor, C. B. Thompson, and S. J. Korsmeyer. 2001. "Proapoptotic BAX  
538 and BAK: A Requisite Gateway to Mitochondrial Dysfunction and Death." *Science* 292  
539 (5517): 727–30. <https://doi.org/10.1126/science.1059108>.
- 540 Wiley, Steven R., Ken Schooley, Pamela J. Smolak, Wenie S. Din, Chang Pin Huang, Jillian K.  
541 Nicholl, Grant R. Sutherland, et al. 1995. "Identification and Characterization of a New  
542 Member of the TNF Family That Induces Apoptosis." *Immunity* 3 (6): 673–82.  
543 [https://doi.org/10.1016/1074-7613\(95\)90057-8](https://doi.org/10.1016/1074-7613(95)90057-8).
- 544 Xu, Daqian, Zheng Wang, Yuxue Zhang, Wei Jiang, Yi Pan, Bao-Liang Song, and Yan Chen.  
545 2015. "PAQR3 Modulates Cholesterol Homeostasis by Anchoring Scap/SREBP Complex  
546 to the Golgi Apparatus." *Nature Communications* 6 (1). Nature Publishing Group: 8100.  
547 <https://doi.org/10.1038/ncomms9100>.
- 548 Yamaguchi, Hirohito, and Hong-Gang Wang. 2004. "CHOP Is Involved in Endoplasmic  
549 Reticulum Stress-Induced Apoptosis by Enhancing DR5 Expression in Human Carcinoma  
550 Cells." *The Journal of Biological Chemistry* 279 (44). American Society for Biochemistry  
551 and Molecular Biology: 45495–502. <https://doi.org/10.1074/jbc.M406933200>.
- 552

553 **Figure Legends**554 **Fig 1. Misfolded proteins induce DR5-dependent apoptosis and assemble DR5-caspase 8**  
555 **signaling complexes.**

- 556 A) Confocal images of epithelial cells HCT116 fixed 24 h post-transfection with 0.25-1.0  $\mu\text{g}$   
557 of a plasmid containing myelin protein zero (MPZ) tagged with a C-terminal monomeric  
558 EGFP or 1.0  $\mu\text{g}$  of the empty vector showing MPZ-GFP fluorescence (green) and  
559 immunofluorescence with an antibody against DR5 (red) (scale bar = 5  $\mu\text{m}$ ).
- 560 B) Western blot of HCT116 cell lysates harvested 24 h post-transfection with a titration of  
561 MPZ-GFP plasmid or the empty vector (C8 = caspase 8, cC3 = cleaved caspase 3). p55  
562 represents full-length, inactive C8; p43 indicates a C8 intermediate after release of the  
563 active p10 subunit, and p29 corresponds to the released p18 and p10 subunits.
- 564 C) Western blot of HCT116 cells transfected with siRNA against a non-targeting (Nt) control  
565 or DR5 (48 h) followed by the empty vector +/- 100 nM thapsigargin (Tg), 1.0  $\mu\text{g}$  MPZ-  
566 GFP, or cytosolic GFP (24 h; \* denotes degradation products; L and S denote the long  
567 and short isoforms of DR5, respectively; FL and C denote full-length and cleaved PARP,  
568 respectively).
- 569 D) Average percent of annexin V staining for HCT116 cells transfected as described in C)  
570 from  $n = 3$  biological replicates (error bars = SEM; \* indicates  $p < 0.05$ ; ns indicates  $p =$   
571 0.46 as analyzed by unpaired t-test with equal SD). See Fig 1–figure supplement 4D for  
572 gating.
- 573 E) Top: Caspase 8 activity in size exclusion chromatography fractions from lysates of  
574 HCT116 cells transfected with 1.0  $\mu\text{g}$  MPZ-GFP or cytosolic GFP (24 h). Bottom: Size  
575 exclusion fractions were pooled according to dotted grid lines and immunoblotted for  
576 DR5 and GFP (\* denotes degradation products).

577 F) Immunoprecipitation of GFP-tagged proteins from lysates of HCT116 transfected with  
578 MPZ-GFP, cytosolic GFP, or the empty vector (L and S denote the long and short  
579 isoforms of DR5, respectively). The percent of total DR5 recovered has been quantified  
580 in Figure 1–figure supplement 5C.

581 G) Fold change in caspase 8 activity relative to the empty vector control for beads with  
582 immunoprecipitated contents shown in Fig 1F (error bars = SEM for n = 3 biological  
583 replicates; \* indicates p = 0.023 and ns indicates p = 0.83 as calculated by unpaired t-  
584 tests with equal SD).

585

586 **Fig 1–source data 1: FCS files and quantification of Annexin V staining for MPZ-GFP**

587 This zip archive contains FCS files from n = 3 biological replicates of HCT116 transfected with  
588 the conditions outlined in Fig 1D. The excel file contains the quantification of Annexin V staining  
589 exported from FlowJo.

590

591 **Fig 1–source data 2: Caspase glo 8 measurements for IP of MPZ-GFP vs GFP**

592 This zip archive contains the measured luminescent units for caspase glo 8 activity shown in  
593 Figures 1G (IP beads) and Fig 1S3C (input lysates). Coomassie gels used to normalize lysate  
594 concentration are included as .tif files.

595

596

597



598 **Fig 1–figure supplement 1: Sustained MPZ-GFP expression invokes a terminal, pro-**  
599 **apoptotic UPR at late time points.**

600 A) qPCR for reverse-transcribed transcripts harvested from HCT116 cells transfected with  
601 0.12-1.0  $\mu\text{g}$  of a plasmid containing myelin protein zero (MPZ) tagged with a C-terminal  
602 monomeric EGFP or 1.0  $\mu\text{g}$  of the empty vector for 24 h (n = 3 technical replicates, error  
603 bars = SD; \* denotes  $p < 0.05$  as analyzed by multiple t-tests with Holm-Sidak correction  
604 for multiple comparisons).

605 B) Quantification of the mean intensity for DR5 versus the mean intensity of intracellular  
606 MPZ-GFP per cell for HCT116 transfected with 0.25  $\mu\text{g}$  (left) and 1.0  $\mu\text{g}$  (right) of MPZ-  
607 GFP plasmid to show the correlation between DR5 and MPZ-GFP expression levels per  
608 cell. Intensity values given by CellProfiler algorithms were normalized to 0.02 for DR5  
609 and 0.06 for MPZ-GFP to assign arbitrary values. P values were calculated from  
610 unpaired two-tailed t-tests.

611 C) RT-PCR for unspliced and spliced forms of *Xbp1* mRNA isolated from HCT116 cells  
612 transfected for 24 h with the empty vector or for various time points with 1  $\mu\text{g}$  MPZ-GFP,  
613 followed by cells treated with 100 nM Tg for 2 h and 24 h.

614 D) Western blot of HCT116 cell lysates harvested 24 h post-transfection with the empty  
615 vector, or 3-24 h post-transfection with 1  $\mu\text{g}$  MPZ-GFP.

616 E) Fold change in caspase 8 activity, as measured by a luminescent caspase 8 substrate,  
617 of lysates from HCT116 harvested 3-24 h post-transfection with 1  $\mu\text{g}$  MPZ-GFP relative  
618 to cells transfected with the empty vector control (error bars represent SD of n = 3  
619 technical replicates; \*\*\* denotes  $p < 0.005$ , and ns indicates  $p = 0.15$  by unpaired t-test  
620 with equal SD).

621  
622

623

624 **Fig 1–source data 3: qPCR analysis of MPZ-GFP titration**

625 This zip archive contains the compiled excel file for qPCR data shown in Fig 1–figure  
626 supplement 1A along with the Prism 6 file used to perform multiple t-tests with Holm-Sidak  
627 correction for multiple comparisons

628

629 **Fig 1–source data 4: Caspase glo 8 measurements for time course of MPZ-GFP**

630 **transfection**

631 This zip archive contains the measured luminescent units for caspase glo 8 activity shown in  
632 Figures 1–figure supplement 1E and the tif file of the Coomassie blue-stained gel used to  
633 normalize lysate concentrations.

634

635 **Fig 1–figure supplement 2: Upregulating DR5 levels in the absence of ER stress through**  
636 **ectopic expression of CHOP is not sufficient to induce apoptosis.**

- 637 A) Western blot of HCT116 cell lysates harvested 24 h post-transfection with a titration of  
638 0.03-0.50  $\mu$ g of a CHOP expression vector, 1  $\mu$ g MPZ-GFP plasmid, or the empty vector  
639 (FL = full-length, C = cleaved).
- 640 B) qPCR for reverse-transcribed transcripts harvested from HCT116 cells transfected with  
641 0.03-0.50  $\mu$ g of a CHOP expression vector, 1.0  $\mu$ g of MPZ-GFP, or 1.0  $\mu$ g of the empty  
642 vector for 24 h (n = 3 technical replicates, error bars = SD, \* denotes p < 0.05).
- 643 C) Representative images of automated counting for Trypan blue-stained cells, where  
644 green outlines denote non-stained (live) cells and red outlines denote stained cells  
645 (Trypan blue+, dead).
- 646 D) Average percentage of cells transfected as described in (S3A) stained with Trypan blue  
647 as quantified by automated cell counting from n = 3 biological replicates (error bars =  
648 SEM; \*\* denotes p = 0.008 and ns = non-significant for unpaired t-test with equal SD; ns<sup>1</sup>  
649 refers to p = 0.19 from unpaired t-test with Welch's correction for variance).

650  
651 **Fig 1–source data 5: qPCR and cell death measurement for CHOP expression**

652 This zip archive contains the qPCR analysis from CHOP expression in Fig 1–figure supplement  
653 2B, and brightfield images of Trypan Blue staining measured on the Countess II for n = 3  
654 biological replicates, summarized in Fig 1–figure supplement 2D.

655

656 **Fig 1–figure supplement 3: DR5 immunoprecipitates with FADD and MPZ-GFP.**

657 A) Immunoprecipitation of DR5 from HCT116 transfected with MPZ-GFP or the empty  
658 vector and blotted for DR5, MPZ-GFP, and FADD.

659 B) Inputs for GFP pulldown performed in Fig. 1F.

660 C) Caspase 8 activity of inputs relative to the empty vector control for the GFP pulldown  
661 performed in Fig 1F (n = 3 biological replicates, error bars = SEM, \*\* indicates p =  
662 0.0046, and \* indicates p < 0.05 from unpaired t-tests with equal SD). Source data can  
663 be found in Figure 1–source data 2.

664

665

666

667

668

669

- 670 **Fig 1–figure supplement 4: Sustained overexpression of other ER-trafficked proteins**  
671 **induce UPR-mediated apoptosis in a DR5-dependent manner.**
- 672 A) qPCR for reverse-transcribed transcripts harvested from HCT116 cells transfected with  
673 1.0  $\mu\text{g}$  of GFP-tagged rhodopsin (RHO), proinsulin (INS), or 1.0  $\mu\text{g}$  of the empty vector  
674 for 24 h (n = 2 biological replicates, each with 3 technical replicates; error bars = SD; \*  
675 denotes  $p < 0.05$ ).
- 676 B) RT-PCR for unspliced and spliced forms of *Xbp1* mRNA isolated from HCT116 cells  
677 transfected for 24 h with 1  $\mu\text{g}$  of empty vector +/- 100 nM Tg for 2 h, MPZ-GFP, INS-  
678 GFP, or RHO-GFP.
- 679 C) Western blot of HCT116 cells transfected with siRNA against a non-targeting (Nt) control  
680 or DR5 (48 h) followed by 1.0  $\mu\text{g}$  RHO-GFP or INS-GFP (24 h).
- 681 D) Representative flow cytometry histograms of HCT116 cells transfected with the listed  
682 siRNA and vector and stained with annexin V-AlexaFluor647. Y-axis has been scaled so  
683 that the mode = 100%. Dotted lines represent gating to distinguish staining-positive  
684 cells. Left: Histograms of fluorescence at 647 nm to measure annexin V staining. Right:  
685 Histograms of fluorescence at 488 nm to compare level and distribution of GFP-tagged  
686 protein expression. To note, GFP expression profiles for the same construct are similar  
687 between different siRNA transfected samples.
- 688 E) Average percent of Annexin V-positive cells for HCT116 cells transfected with siRNA  
689 and GFP-tagged rhodopsin/proinsulin (n = 3 biological replicates, error bars = SEM, \*  
690 indicates  $p = 0.011$ , \*\* indicates  $p = 0.005$  from unpaired t-test with equal SD). Gating for  
691 annexin V-positive staining is shown in Fig 1–figure supplement 4D.

692

693

694

695 **Fig 1–source data 6: qPCR analysis of INS and RHO-GFP expression**

696 This zip archive contains the compiled excel file for qPCR data shown in Fig 1–figure  
697 supplement 4A along with the Prism 6 file used to perform multiple t-tests with Holm-Sidak  
698 correction for multiple comparisons.

699

700 **Fig 1–source data 7: FCS files and quantification of Annexin V staining for INS and RHO**

701 This zip archive contains FCS files from n = 3 biological replicates of HCT116 transfected with  
702 the conditions outlined in Fig 1–figure supplement 4E. The excel file contains the quantification  
703 of annexin V staining exported from FlowJo.

704

705

706 **Fig 1–figure supplement 5: DR5 engages a selective subset of ER-trafficked client**  
707 **proteins upon prolonged ER stress.**

708 A) Pulldown of GFP-tagged proteins from HCT116 transfected with INS, RHO, or cytosolic  
709 GFP. Inputs (left) and immunoprecipitated samples (right) were immunoblotted for GFP  
710 and DR5 (L and S indicate long and short isoforms, respectively).

711 B) Fold change in caspase 8 activity relative to cytosolic GFP for beads with  
712 immunoprecipitated contents described in Fig 1–figure supplement 5A as measured by  
713 caspase glo 8 luminescence (n = 2 biological replicates, error bars = SEM, \* indicates p  
714 < 0.05, \*\* indicates p = 0.0013, \*\*\*\* indicates p < 0.005 from unpaired t-tests with equal  
715 SD).

716 C) Quantification of the percent of total DR5 recovered in the IPs of GFP-tagged proteins,  
717 shown in Fig 1G and Figure 1–figure supplement 5A. (n = 3 biological replicates for GFP  
718 and MPZ, while n = 2 biological replicates for INS and RHO. \* denotes p = 0.016, \*\*  
719 denotes p = 0.0035, and ns denotes p = 0.39 from unpaired t-test with equal SD) The  
720 DR5 signal of the input and IP lanes were quantified from the same exposure and then  
721 normalized to the amount loaded on the gel. Source data of blots and quantification are  
722 provided in Fig 1–source data 9.

723

724 **Fig 1–source data 8: Caspase glo 8 measurements for IP of INS and RHO-GFP**

725 This zip archive contains the measured luminescent units for caspase glo 8 activity shown in  
726 Figures 1S5B (input lysates and IP beads). Coomassie gels used to normalize lysate  
727 concentration are included as .tif files.

728

729 **Fig 1–source data 9: Westerns and quantification of DR5 recovered on IPs**

730 This zip archive contains images of the Western blots and measurements used to quantify the  
731 amount of DR5 in the IP samples relative to the input lysate

732 **Fig 2: Misfolded protein engages DR5 at the ER-Golgi intermediate compartment,**  
733 **inducing active DR5 signaling clusters.**

- 734 A) Top: Immunofluorescence of HCT116 cells transfected with MPZ-GFP (green) for 24 h  
735 and stained with anti-DR5 (red, scale bar 5  $\mu\text{m}$ ). Bottom: Enlargements of the inset  
736 stepping through the z-plane in 0.5  $\mu\text{m}$  increments (scale bar 2  $\mu\text{m}$ ).
- 737 B) Subcellular fractionation of lysate expressing MPZ-GFP, where IRE1 marks the ER,  
738 Giantin marks the Golgi, Sec31A and Sec23A mark COPII vesicles, and ERGIC53 and  
739 RCAS1 correspond to ER-Golgi intermediate compartment. Bands of the expected size  
740 are indicated by “–” and bands that may represent a modified or degraded protein are  
741 indicated by \*.
- 742 C) Average caspase activity of each fraction from subcellular gradient centrifugation in (B)  
743 normalized to total lysate (input) measured by caspase 8 substrate luminescence (n = 3  
744 biological replicates, error bars = SEM; ns<sup>1</sup> indicates p = 0.079, \* denotes p = 0.015, and  
745 ns indicates p = 0.31 from unpaired t-tests with equal SD).
- 746 D) Top: Immunostaining of DR5 and ERGIC53 in fixed HCT116 cells transfected with MPZ-  
747 GFP for 24 h as in (A). Bottom: Merged images with ERGIC53 in magenta or cyan to  
748 depict overlapping signal as white (scale bar = 5  $\mu\text{m}$ , insets scale bar = 2  $\mu\text{m}$ ).
- 749 E) Immunostaining of DR5 and giantin in fixed HCT116 cells expressing MPZ-GFP. Giantin  
750 is magenta in the overlay with MPZ (green) or cyan in the overlay with DR5 (red).  
751 Bottom row enlarges the inset marked in the merges images to show little overlapping  
752 signal with Giantin (scale bar = 5  $\mu\text{m}$ , inset scale bar = 1  $\mu\text{m}$ ).
- 753 F) Box-whisker plots quantifying the Pearson’s correlation per cell between DR5 and  
754 ERGIC53 (mean =  $0.61 \pm 0.03$ ) or Giantin (mean =  $0.14 \pm 0.02$ ) within MPZ-positive  
755 cells (N > 55), where whiskers correspond to minimum and maximum values of the data  
756 (\*\*\*\* indicates p < 0.001).



757 **Fig 2—source data 1: Caspase activity for fractions of iodixanol gradient**

758 This excel file contains the caspase glo 8 luminescent units of the fractionation samples (n = 3  
759 biological replicates) shown in Fig 2C.

760 **Fig 2–figure supplement 1: Intracellular puncta of overexpressed MPZ and rhodopsin**  
761 **proteins show significant co-localization with DR5 clusters.**

- 762 A) Immunofluorescence of fixed HCT116 cells transfected with siRNA (left: non-targeting,  
763 right: siDR5) for 48 h and MPZ-GFP (green in merge) for 24 h and subsequently  
764 immunostained for anti-DR5 (red in merge). Two representative confocal images are  
765 shown for each siRNA treatment, where the scale bar corresponds to 5  $\mu\text{m}$ .
- 766 B) Immunofluorescence of fixed HCT116 cells expressing RHO-GFP for 24 h and stained  
767 for DR5 and GFP (scale bar = 5  $\mu\text{m}$ , inset scale bar = 2  $\mu\text{m}$ ).
- 768 C) Quantification of Pearson's correlation per cell between DR5 signal and ER-trafficked  
769 protein (MPZ and RHO) 24 h-post transfection from original image files versus artificially  
770 rotated image files, for which the GFP channel was rotated  $90^\circ$  with respect to the other  
771 channel. Whisker-box plots depict the Tukey method. Statistics were performed through  
772 unpaired two-tailed t-tests, where \*\*\*\* indicates  $p < 0.0001$  and the variance was non-  
773 significant.
- 774 D) Immunofluorescence for DR5 and RCAS1 in fixed HCT116 cells expressing MPZ-GFP.  
775 RCAS1 is magenta in the overlay with MPZ (green) or cyan in the overlay with DR5  
776 (red), where white puncta signify co-localized signal (scale bar = 5  $\mu\text{m}$ , inset scale bar =  
777 1  $\mu\text{m}$ ).

778 **Fig 2–figure supplement 2: Misfolded protein accumulation in the ERGIC precedes DR5**  
779 **retention in the ERGIC.**

780 A) Immunofluorescence for DR5 and ERGIC53 in HCT116 fixed 20 hr post-transfection.

781 ERGIC53 is magenta in the overlay with MPZ (green) or cyan in the overlay with DR5

782 (red) (scale bar = 5  $\mu\text{m}$ ). Arrows in inset images depict regions where MPZ and

783 ERGIC53 signal overlap (scale bar = 2  $\mu\text{m}$ ).

784 B) Quantification of Pearson's correlation per cell between ERGIC and MPZ, or Giantin and

785 MPZ of fixed HCT116 cells at the specified time after MPZ-GFP transfection. Whisker-

786 box plots depict the Tukey method. Statistics were performed through unpaired two-

787 tailed t-tests, where \*\*\*\* indicates  $p < 0.001$  and ns means not significant, and the

788 variance was non-significant.

789 C) Quantification of Pearson's correlation per cell between DR5 signal and ERGIC53 of

790 fixed HCT116 cells at 20 h and 24 h post-transfection with MPZ-GFP. Whisker-box plots

791 depict the Tukey method. Statistics were performed through unpaired two-tailed t-tests,

792 where \*\*\*\* indicates  $p < 0.001$  and the variance was non-significant.

793 **Fig 3: Direct binding of exposed ER-trafficked protein sequences to the DR5 ECD is**  
794 **sufficient to induce oligomerization.**

- 795 A) A peptide array tiled with sequences from the ectodomain of myelin protein zero (MPZ)  
796 and extracellular loops from rhodopsin (RHO) was incubated with Fc-tagged DR5  
797 ectodomain domain (long isoform, 500 nM). Signal was obtained by probing with anti-Fc.
- 798 B) Coomassie stained SDS-PAGE gel of pulldown on Fc-tagged DR5L ECD (55 kDa) or  
799 TNFR1 ECD (65 kDa) incubated with increasing concentrations of the MPZ-ecto<sup>VD</sup>  
800 peptide (apparent MW of 10 kDa, see Table S5 for sequence).
- 801 C) Fluorescence quenching of AlexaFluor647-DR5L (green) or TNFR1 ECD (blue) was  
802 measured with increasing MPZ-ecto peptide to quantify the binding affinity, whereas  
803 quenching was not observed with the mutated MPZ-ecto<sup>Tyr→Glu</sup> peptide (magenta) (N=3,  
804 error bars are SD). DR5L ECD binds to the MPZ-ecto peptide with a  $K_{1/2}$  of  $109 \pm 11 \mu\text{M}$   
805 with a hill coefficient of  $2.6 \pm 0.5$ .
- 806 D) SDS-PAGE of recombinant FLAG-tagged DR5L ECD (25 kDa, 10  $\mu\text{M}$ ) incubated with  
807 MPZ-ecto peptide at the noted concentrations and treated with the amine crosslinker  
808 BS3 (100  $\mu\text{M}$ ), probed with anti-FLAG.
- 809 E) Size exclusion chromatographs of absorbance at 280 nm for 25  $\mu\text{M}$  recombinant DR5L  
810 ECD alone (black), pre-incubated with 100  $\mu\text{M}$  fluorescein-conjugated MPZ-ecto peptide  
811 (green) or 100  $\mu\text{M}$  fluorescein-conjugated MPZ-ecto<sup>Tyr→Glu</sup> peptide (magenta).
- 812 F) SDS-PAGE gels scanned for fluorescence and then stained with Coomassie for eluted  
813 size exclusion fractions in (E). Green outlines (top pair) correspond to fractions from  
814 DR5L pre-incubated with MPZ-ecto peptide, and magenta outlines (bottom pair)  
815 correspond to DR5L with MPZ-ecto<sup>Tyr→Glu</sup> peptide. Lane marked by “-“ denotes a blank  
816 lane between the input and 7-ml fraction to minimize spillover of signal from input  
817 sample. Arrowheads mark detectable peptide fluorescence in the indicated fractions.

818 **Fig 3—figure supplement 1: DR5 ECD binds to selective subset of sequences displayed**  
819 **by the secretory proteome.**

820 A) Intensity values of each peptide spot in the MPZ section of the peptide array in Fig 3A  
821 were normalized to the spot of highest intensity within MPZ. Green box below denotes  
822 the peptide chosen as a candidate binder, called MPZ-ecto, shown in spots C18-C19 on  
823 the array. Sequences for the peptides are listed in Fig 3—source data 1.

824 B) Intensity values of the RHO peptide array section in Fig 3A normalized to the highest  
825 intensity from MPZ. Peptides were derived from the extracellular N-terminus tail and the  
826 extracellular loops (EL1-EL3) that connect the transmembrane domains of rhodopsin.

827 C) Quantification of enriched amino acids from peptides with an intensity value greater than  
828 one standard deviation above the average signal, noted as a preferred peptide, within  
829 the entire array. Enrichment ratio for each amino acid was calculated as the frequency of  
830 occurrence in preferred peptides divided by its total frequency on the array.

831

832 **Fig 3—source data 1: Sequences and quantification of peptides probed with Fc-DR5 ECD**  
833 **on the peptide array**

834 This excel file contains the peptide sequences of the peptide array shown in Fig 3A, the  
835 quantification of DR5 ECD detected for each spot, and the analysis for enriched amino acids in  
836 Fig 3—figure supplement 1.

837 **Fig 3—figure supplement 2: Purified recombinant DR5 ECD oligomerizes with peptide in a**  
838 **specific and reversible manner.**

- 839 A) Fluorescence scan at 647 nm of SDS-PAGE for gel filtration-purified DR5L (25 kDa) or  
840 TNFR1 ECD (35 kDa) labeled with NHS-ester AlexaFluor647. These proteins were used  
841 in the fluorescence quenching assays shown in Fig 3C.
- 842 B) Fluorescence de-quenching of AlexaFluor647-DR5L ECD (200 nM) pre-incubated with  
843 100  $\mu$ M or 200  $\mu$ M of MPZ-ecto peptide in the presence of increasing concentrations of  
844 unlabeled DR5L ECD.
- 845 C) Coomassie-stained SDS-PAGE of gel filtration purified FLAG-tagged DR5L ECD  
846 proteins used for the crosslinking assay in Fig 3D and size exclusion chromatography in  
847 Fig 3E.
- 848 D) Size exclusion chromatographs of absorbance at 280 nm for recombinant DR5L ECD to  
849 show that increased concentration of DR5L alone does not yield multimers.
- 850 E) Size exclusion chromatographs of absorbance at 280 nm for recombinant DR5L ECD  
851 alone (25  $\mu$ M, black) or incubated with TRAIL (25  $\mu$ M, purple). Trace for TRAIL alone (50  
852  $\mu$ M) is shown in light orange.
- 853 F) SDS-PAGE gels stained with Coomassie blue for eluted size exclusion fractions in Fig  
854 S8E depicting bands for DR5L ECD and TRAIL.
- 855 G) Size exclusion chromatographs of absorbance at 280 nm for 25  $\mu$ M recombinant DR5L  
856 ECD alone (black), pre-incubated with 400  $\mu$ M fluorescein-conjugated MPZ-ecto peptide  
857 (teal).
- 858 H) SDS-PAGE gels scanned for fluorescence and then stained with Coomassie for eluted  
859 size exclusion fractions in Fig 3—figure supplement 2G. Lane marked by “-“ denotes a  
860 blank lane between the input and 7-ml fraction to minimize spillover of signal from input  
861 sample. Arrowheads mark detectable peptide fluorescence in the indicated fractions.

862 **Fig 4: Disrupting misfolded protein binding to DR5 impairs ER stress-induced apoptosis.**

- 863 A) Diagram of constructs generated to replace the MPZ ectodomain with the minimal DR5-  
864 binding MPZ-ecto peptide (green), the peptide harboring Tyr → Glu mutations  
865 (magenta), or the peptide with all aromatic residues (Arom) mutated to Glu (light pink).  
866 SS = signal sequence of MPZ, TM = transmembrane domain, ICD = intracellular domain.
- 867 B) Western blot of HCT116 cell lysates harvested 24 h post-transfection with 1 μg of MPZ-  
868 GFP plasmid, empty vector, or a titration of GFP-tagged MPZ-ecto peptide variants,  
869 followed by GFP alone. FL denotes full-length PARP, while C denotes cleaved PARP.  
870 The percentage of cleaved PARP was calculated as the signal of cleaved PARP divided  
871 by total PARP (FL + C). Arrows denote conditions carried forward for normalized  
872 expression levels of the ecto peptide constructs.
- 873 C) Fold change in caspase 8 activity relative to GFP expression, as measured by  
874 incubation of luminescent caspase glo 8 substrate with lysates from HCT116 transfected  
875 using conditions described in Fig 4B lanes 5, 7 and 10 (error bars represent SEM of n =  
876 3 biological replicates; \*\*\* denotes p < 0.005, and ns indicates p = 0.18 from unpaired t-  
877 tests with equal SD).
- 878 D) RT-PCR for unspliced and spliced forms of *Xbp1* mRNA isolated from HCT116 cells  
879 transfected for 24 h with the empty vector +/- 100 nM Tg, or with MPZ-GFP, or MPZ-ecto  
880 peptide GFP and its mutant variants (Tyr → Glu and Arom → Glu) using conditions from  
881 Fig 4B, lanes 5, 7, and 10.
- 882 E) qPCR for reverse-transcribed transcripts harvested from HCT116 cells transfected with  
883 the constructs described in 4A, using conditions shown in Fig 4B lanes 5, 7, and 10. (n =  
884 3 biological replicates, \* denotes p < 0.05 and ns = non-significant).

- 885 F) Immunofluorescence for DR5 and ERGIC53 in HCT116 transfected with the MPZ-ecto  
886 peptide for 24 hrs. ERGIC53 is magenta in the overlay with MPZ (green) or cyan in the  
887 overlay with DR5 (red) (scale bar = 5  $\mu$ m).
- 888 G) Left: Immunoblots of HCT116 lysate inputs expressing the constructs described in 4A,  
889 where L and S mark the long and short isoforms of DR5, respectively, and where FL and  
890 C mark the full-length and cleaved fragments of PARP, respectively. The percentage of  
891 cleaved PARP is quantified as the signal of the cleaved fragment divided by total PARP  
892 (FL + C). Right: Immunoprecipitation of GFP-tagged proteins from the lysates shown in  
893 (C), where L and S denote the long and short isoforms of DR5, respectively.
- 894 H) Average percent of annexin V staining for HCT116 cells transfected as described in C)  
895 and D) from n = 3 biological replicates (error bars = SEM, \* indicates p = 0.026, and \*\*  
896 indicates p = 0.003 from unpaired t-tests with equal SD). See Fig 4–figure supplement 3  
897 for distribution of early vs late apoptotic cells.

898

899 **Fig 4–source data 1: Caspase glo 8 measurements for MPZ-ecto peptide expression**

900 This zip archive contains the measured luminescent units for caspase glo 8 activity shown in  
901 Figures 4C (lysates) and the coomassie gel used to normalize lysate concentration as a.tif file.

902

903 **Fig 4–source data 2: qPCR and statistical analysis for expression of MPZ-ecto peptides**

904 This zip archive contains the compiled excel file for qPCR data shown in Fig 4E along with the  
905 Prism 6 file used to perform multiple t-tests with Holm-Sidak correction for multiple comparisons.

906

907 **Fig 4–source data 3: FCS files and quantification of Annexin V staining for MPZ-ecto**  
908 **peptides**



909 This zip archive contains FCS files from  $n = 3$  biological replicates of HCT116 transfected with  
910 the conditions outlined in Fig 4H. The excel file contains the quantification of Annexin V staining  
911 exported from FlowJo.  
912

913 **Fig 4—figure supplement 1: Introducing Glu mutations to the DR5-binding sequence of**  
914 **MPZ disrupts PARP cleavage in a DR5-dependent manner.**

915 A) Western blot of HepG2 cell lysates harvested 24 h post-transfection with 1  $\mu$ g of the  
916 empty vector, MPZ-GFP, or a titration of GFP-tagged MPZ-ecto peptide variants. FL  
917 denotes full-length PARP, while C denotes cleaved PARP. The percentage of cleaved  
918 PARP was calculated as the signal of cleaved PARP divided by total PARP (FL + C).

919 B) Western blot of HCT116 cell lysates transfected with siRNA against a non-targeting (Nt)  
920 sequence or DR5 (referred to as DR5-siRNA-2 in Materials and Methods) for 48 h and  
921 co-expressing FLAG-tagged DR5 long isoform and/or MPZ-ecto peptide-GFP.

922

923 **Fig 4—figure supplement 2: Glu-containing mutants of MPZ-ecto peptide accumulate in**  
924 **the ERGIC.**

925 A) Immunofluorescence for DR5 and ERGIC53 in HCT116 transfected with the MPZ-ecto  
926 Tyr-to-Glu peptide for 24 hrs. ERGIC53 is magenta in the overlay with MPZ (green) or  
927 cyan in the overlay with DR5 (red) (scale bar = 5  $\mu$ m).

928 B) Immunofluorescence for DR5 and ERGIC53 in HCT116 transfected with the MPZ-ecto  
929 Arpm-to-Glu peptide for 24 hrs. ERGIC53 is magenta in the overlay with MPZ (green) or  
930 cyan in the overlay with DR5 (red) (scale bar = 5  $\mu$ m).

931 C) Quantification of Pearson's correlation per cell between ERGIC53 and GFP-tagged  
932 peptides of fixed HCT116 cells at 24 h post-transfection with MPZ-ecto peptide (green)  
933 and the Glu-containing peptide mutants (dark and light pink). Whisker-box plots depict  
934 the Tukey method. Statistics were performed through unpaired two-tailed t-tests, where  
935 ns indicates  $p > 0.50$ .

936 D) Quantification of Pearson's correlation per cell between DR5 and GFP-tagged peptides  
937 of fixed HCT116 cells at 24 h post-transfection with MPZ-ecto peptide (green) and the  
938 Glu-containing peptide mutants (dark and light pink). Whisker-box plots depict the Tukey  
939 method. Statistics were performed through unpaired two-tailed t-tests with equal SD,  
940 where ns means  $p > 0.11$ .

941 E) Table summarizing the mean  $\pm$  SEM of the Pearson's correlation per cell shown in  
942 Whisker-box plots of C-D.

943

944

945

946

947 **Fig 4—figure supplement 3: MPZ-ecto peptide engagement of DR5 in cells drives**  
948 **apoptotic cell death.**

- 949 A) Quantification of the percent of total DR5 recovered in the IPs of GFP-tagged MPZ-ecto  
950 peptides, shown in Fig 4G. (n = 2 biological replicates. \* denotes p = 0.047, \*\* denotes p  
951 = 0.0054, and ns indicates p = 0.62 from unpaired t-test with equal SD.) The DR5 signal  
952 of the input and IP lanes were quantified from the same exposure and then normalized  
953 to the amount loaded on the gel. Source data of blots and quantification are provided in  
954 Fig 4—source data 4.
- 955 B) Flow cytometry measurements of SytoxBlue (405 nm) and annexin V (647 nm) staining  
956 of HCT116 transfected with empty vector for 24 h.
- 957 C) Flow cytometry measurements of SytoxBlue (405 nm) and annexin V (647 nm) staining  
958 of HCT116 transfected with GFP-tagged MPZ-ecto peptide for 24 h.
- 959 D) Flow cytometry measurements of SytoxBlue (405 nm) and annexin V (647 nm) staining  
960 of HCT116 transfected with GFP-tagged MPZ-ecto peptide and co-treated with 20  $\mu$ m of  
961 z-VAD for 24 h.
- 962 E) Flow cytometry measurements of SytoxBlue (405 nm) and annexin V (647 nm) staining  
963 of HCT116 transfected with GFP-tagged MPZ-ecto Tyr→Glu peptide for 24 h.
- 964 F) Flow cytometry measurements of SytoxBlue (405 nm) and annexin V (647 nm) staining  
965 of HCT116 transfected with GFP-tagged MPZ-ecto Arom→Glu peptide for 24 h.
- 966 G) Table summarizing percent of cells stained in each quadrant of plots shown in B-F.

967

968 **Fig 4—source data 4: Westerns and quantification of DR5 recovered on IPs**

969 This zip archive contains .tif files of the Westerns from inputs and IPs of the MPZ-ecto peptides  
970 (n = 2 biological replicates) used to quantify the percent of DR5 recovered shown in Fig 4—figure  
971 supplement 3A.

972

973 **Acknowledgements**

974 We thank D. Lawrence at Genentech for gifting anti-DR5 5C7-conjugated agarose beads and  
975 helpful discussions. We are grateful to C.M. Gallagher for her detailed immunofluorescence  
976 protocols, to G.E. Karagöz for her insight on peptide binding assays, to N.W. Frankel for his  
977 help in flow cytometry, to K. Crotty for her quantitative PCR protocol, and to S. Mukherjee for  
978 her thoughtful feedback. M. Lam was funded by a National Science Foundation Graduate  
979 Research fellowship. S. Marsters is Principal Staff Researcher and A. Ashkenazi is Senior Staff  
980 Scientist of Genentech, Inc. P. Walter is an investigator of the Howard Hughes Medical Institute.

981 **Materials & Methods**

982

<b>Key Resources Table</b>				
<b>Reagent type (species) or resource</b>	<b>Designation</b>	<b>Source or reference</b>	<b>Identifiers</b>	<b>Additional information</b>
Gene ( <i>Homo-sapiens</i> )	DR5		O14763 (TR10B_HUMAN)	
Gene ( <i>Homo-sapiens</i> )	INS (proinsulin)		P01308 (INS_HUMAN)	
Gene ( <i>Homo-sapiens</i> )	MPZ (myelin protein zero)		P25189 (MYP0_HUMAN)	
Gene ( <i>Homo-sapiens</i> )	RHO (rhodopsin)		P08100 (OPSD_HUMAN)	
cell line ( <i>Homo-sapiens</i> )	HCT116	ATCC	CCL-247	
cell line ( <i>Homo-sapiens</i> )	HepG2	ATCC	CRL-10741	
Transfected construct ( <i>homo sapiens</i> )	CHOP (canonical isoform)	this paper		expression of CHOP in absence of ER stress used in Figure 1 – fig sup 2
Transfected construct ( <i>homo sapiens</i> )	cytosolic GFP	this paper		expression of GFP used in Figure 1C-1H

Transfected construct ( <i>homo sapiens</i> )	DR5 long FLAG-His6x, WT with silent mutation	this paper		expression of DR5 long isoform-FLAG, harbors silent nt mutations within signal sequence to evade siRNA (AAGACCCTTGTGCTCGTTGTC à AAaACaCTTGTGCTCGTTGTC) used in Figure 4 – fig sup 1
Transfected construct ( <i>homo sapiens</i> )	DR5siRNA-2	Dharmacon	siRNA	AAG ACC CUU GUG CUC GUU GUC UU, knockdown in Fig S9B
Transfected construct ( <i>homo sapiens</i> )	empty vector (no GFP)	this paper		empty vector used in Figure 1, 4B, 4E
Transfected construct ( <i>homo sapiens</i> )	MPZ-ecto peptide-eGFP	this paper		expression of MPZ-ecto peptide (FTWRYQPEGGRDAI SIFHYA) used in Figure 4
Transfected construct ( <i>homo sapiens</i> )	MPZ-ecto peptide <sup>Arom→Glu</sup> -eGFP	this paper		expression of MPZ-ectoArom→Glu peptide (ETEREQPEGGRDAI SIEHEA) used in Figure 4
Transfected construct ( <i>homo sapiens</i> )	MPZ-ecto peptide <sup>Tyr→Glu</sup> -eGFP	this paper		expression of MPZ-ectoTyr→Glu peptide (FTWREQPEGGRDAI SIFHEA) used in Figure 4
Transfected construct ( <i>homo sapiens</i> )	MPZ-eGFP	this paper		expression of MPZ used in Figure 1, 2, 4E

Transfected construct ( <i>homo sapiens</i> )	Nt siRNA	Dharmacon	siRNA	AAA CCU UGC CGA CGG UCU ACC UU
Transfected construct ( <i>homo sapiens</i> )	ON-TARGETplus Human TNFRSF10B 8795 siRNA	Dharmacon	L-004448-00- 0005	Fig 1 knockdowns
Transfected construct ( <i>homo sapiens</i> )	ON-TARGETplus Non-targeting siRNA #2	Dharmacon	D-001810-02-05	Fig 1 knockdowns
Transfected construct ( <i>homo sapiens</i> )	proinsulin (INS) - GFP	this paper		expression of INS- GFP used in Figure 1 – fig sup 4 and 5
Transfected construct ( <i>homo sapiens</i> )	rhodopsin (RHO) -GFP	this paper		expression of RHO- GFP used in Figure 1 – fig sup 4 and 5, 2 — fig sup 1
antibody	anti-caspase 3 (rabbit)	Cell Signaling Technology	9662	1:1000 for Westerns
antibody	anti-caspase 8 5F7 (mouse)	MBL International	M032-3	1:1000 for Westerns
antibody	anti-cleaved caspase 8 (Asp391) (18C8) (rabbit)	Cell Signaling Technology 9496	9496	1:50 for IF fixed with 4% PFA
antibody	anti-DR5 (rabbit)	Cell Signaling Technology	8074	1:1000 for Westerns
antibody	anti-DR5 3H3 (mouse)	Genentech		1:100 for IF fixed with 4% PFA



antibody	anti-ERGIC53 (rabbit)	Sigma Aldrich	E1031	1:1000 for Westerns
antibody	anti-ERGIC53 (rabbit)	Sigma Aldrich E1031	E1031	1:100 for IF fixed with methanol
antibody	anti-FADD (mouse)	BD Biosciences	610400	1:1000 for Westerns
antibody	anti-Fc (mouse)	One World Lab	#603-510	1:1000 for Westerns
antibody	anti-FLAG M2 (mouse)	Sigma	F1804	1:1000 for Westerns
antibody	anti-GAPDH (rabbit)	Abcam	9485	1:1000 for Westerns
antibody	anti-GFP (mouse)	Roche	11814460001	1:1000 for Westerns
antibody	anti-Giantin (rabbit)	Abcam	ab24586	1:1000 for Westerns
antibody	anti-Giantin (rabbit)	Abcam ab24586	ab24586	1:1000 for IF fixed with methanol
antibody	anti-His 6x (mouse)	Abcam	ab15149	1:1000 for Westerns
antibody	anti-IRE1 14C10 (rabbit)	Cell Signaling Technology	3294	1:1000 for Westerns
antibody	anti-mouse- AlexaFluor546	Invitrogen	A11030	1:1000 for IF, centrifuged at 15000xg for 20 mins at 4°C to remove aggregates
antibody	anti-PARP (rabbit)	Cell Signaling Technology	9542	1:1000 for Westerns
antibody	anti-rabbit- AlexaFluor633	Invitrogen	A21071	1:1000 for IF, centrifuged at 15000xg for 20 mins at 4°C to remove aggregates
antibody	anti-RCAS1 D2B6N XP (rabbit)	Cell Signaling Technology	12290	1:1000 for Westerns
antibody	anti-RCAS1 D2B6N XP (rabbit)	Cell Signaling Technology 12290	12290	1:200 for IF fixed with methanol
antibody	anti-Sec23A (rabbit)	Invitrogen	PA5-28984	1:1000 for Westerns
antibody	anti-Sec31A (mouse)	BD Biosciences	612350	1:1000 for Westerns

recombinant DNA reagent	Gp64-His6x-DR5 long ECD pFastBacHT	this paper	plasmid	recombinant protein expression in SF21, used in Figure 3
recombinant DNA reagent	Gp64-His6x-DR5 long ECD-FLAG pFastBacHT	this paper	plasmid	recombinant protein expression in SF21, used in Figure 3
recombinant DNA reagent	Gp64-His6x-TNFR1 ECD pFastBacHT	this paper	plasmid	recombinant protein expression in SF21, used in Figure 3
sequence-based reagent	BiP (GRP78)	this paper	5' primer	GTTCGTGGCGCCTT GTGAC
sequence-based reagent	BiP (GRP78)	this paper	3' primer	CATCTTGCCAGCCA GTTGGG
sequence-based reagent	CHOP (DDIT3)	this paper	5' primer	AGCCAAAATCAGAG CTGGAA
sequence-based reagent	CHOP (DDIT3)	this paper	3' primer	TGGATCAGTCTGGA AAAGCA
sequence-based reagent	DR5 (TNFRSF10B)	this paper	5' primer	TTCTGCTTGCGCTG CACCAGG
sequence-based reagent	DR5 (TNFRSF10B)	this paper	3' primer	GTGCGGCACTTCCG GCACAT
sequence-based reagent	GADD34	this paper	5' primer	GAGGAGGCTGAAGA CAGTGG
sequence-based reagent	GADD34	this paper	3' primer	AATTGACTTCCCTGC CCTCT

sequence-based reagent	GAPDH	this paper	5' primer	AGCCACATCGCTCA GACAC
sequence-based reagent	GAPDH	this paper	3' primer	TGGAAGATGGTGAT GGGATT
sequence-based reagent	GFP	this paper	5' primer	CTGACCTACGGCGT GC
sequence-based reagent	GFP	this paper	3' primer	CCTTGAAGAAGATG GTGCG
sequence-based reagent	MPZ	this paper	5' primer	GGCCATCGTGGTTT ACAC
sequence-based reagent	MPZ	this paper	3' primer	GATGCGCTCTTTGA AGGTC
sequence-based reagent	XBP1 splicing		5' primer	GGAGTTAAGACAGC GCTTGG
sequence-based reagent	XBP1 splicing		3' primer	ACTGGGTCCAAGTT GTCCAG
peptide, recombinant protein	Fc-tagged DR5 ECD	Genentech	recombinant protein	
peptide, recombinant protein	Fc-tagged TNFR1 ECD	Genentech	recombinant protein	

peptide, recombinant protein	MPZ-ecto	Genscript	purified peptide (>95%)	FTWRYQPEGGRDAI SIFHYA
peptide, recombinant protein	MPZ-ecto <sup>Tyr→Glu</sup>	Genscript	purified peptide (>95%)	FTWREQPEGGRDAI SIFHEA
peptide, recombinant protein	MPZ-ecto <sup>VD</sup>	Genscript	purified peptide (>95%)	VSDDISFTWRYQPEG <u>GRD</u>
chemical compound, drug	32% paraformaldehyd e	Electron Microscopy Sciences		fixed with 4% PFA diluted directly into media
chemical compound, drug	AlexaFluor647 NHS Ester (Succinimidyl Ester)	Life Technologies	A37573	fluorescent protein labeling
chemical compound, drug	Annexin V- AlexaFluor 647 conjugate	ThermoFisher	#A23204	apoptosis assays
chemical compound, drug	BS3 (bis(sulfosuccini midyl)suberate)	ThermoFisher	21580	100 μM BS3 for 20 min at RT
chemical compound, drug	Cellfectin II	ThermoFisher	10362100	insect cell expression
chemical compound, drug	Collagen IV	Sigma Aldrich	C6745	0.03 mg/ml in PBS incubated on glass slide for 30 min at RT, and then rinsed off with PBS x 4
chemical compound, drug	DAPI	Molecular Probes	D-1306	5 ug/ml

chemical compound, drug	iQ SYBR Green Supermix	BioRad	#17088800	qPCR
chemical compound, drug	Lipofectamine-LTX	Life Technologies	#15338100	
chemical compound, drug	OptiPrep™ Density Medium	Sigma Aldrich	D1556	iodixanol gradient
commercial assay, kit	caspase glo 8 reagent	Promega	PRG8200	
software, algorithm	CellProfiler	<a href="https://cellprofiler.org/">https://cellprofiler.org/</a>		quantification of mean correlation
commercial assay, kit	Dynabeads Protein G	ThermoFisher	10003D	
software, algorithm	FlowJo	FlowJo, LLC		
commercial assay, kit	GFP-Trap magnetic agarose beads	Chromotek	gtma-20	GFP pulldowns
software, algorithm	Prism 6.0	GraphPad		Kd fits, statistical analyses
other	8-well glass bottom uSlide	Ibidi	80827	
other	normal goat serum	Jackson ImmunoResearch Laboratories	005-000-121	blocked with 2% goat serum diluted into PHEM buffer
other	peptide array	MIT Biopolymers Laboratory	Karagoz et al. 2017	
other	premium capillaries	Nanotemper Technologies	#MO-K025	fluorescence quenching assays

other	SuperDex200 10/300 GL	GE Healthcare	28990944	size exclusion column for fractionation
-------	--------------------------	---------------	----------	--

983

984 **Cell culture and experimental reagents**

985 HCT116 cells (ATCC CCL-247) and HepG2 cells (ATCC CRL-10741) were cultured in DMEM  
 986 with high glucose (Sigma D5796) supplemented with 10% FBS (Life technologies # 10082147),  
 987 2 mM L-glutamine (Sigma G2150), 100 U penicillin, and 100 µg/mL streptomycin (Sigma  
 988 P0781). Cells were incubated at 37°C, 5% CO<sub>2</sub> for growth and transfections. All cell lines were  
 989 authenticated by DNA fingerprint STR analysis by the American Type Culture Collection  
 990 (ATCC). All cell lines were visually inspected using DAPI DNA staining and tested negative for  
 991 mycoplasma. Thapsigargin was purchased from Sigma and used at 100 nM in 0.1% DMSO  
 992 unless otherwise indicated.

993

994 **Statistical analyses**

995 Unpaired two-tailed t-tests for data sets were performed using GraphPad Prism 6.0, where the  
 996 variance between two data sets was non-significant, unless otherwise indicated.

997 **Transient transfections for protein expression**

998 For each 6-well sample seeded with 400,000 cells the evening prior to transfection, the final  
 999 transfection mixture put onto the cells was composed of 2 ml OptiMEM I (Thermo Fisher  
 1000 Scientific #31985070), 5 µl of Lipofectamine-LTX (Life Technologies #15338100), 1000 ng of  
 1001 total DNA (supplemented with the empty vector in cases of variable MPZ-GFP). Plasmid  
 1002 preparations were performed fresh for each transfection to maximize reproducibility. Unless  
 1003 otherwise noted, 1.0 µg of plasmid containing GFP-tagged ER-trafficked protein was used, while  
 1004 0.25 µg of GFP supplemented with 0.75 µg of empty vector was sufficient to yield GFP protein  
 1005 levels in excess of ER-trafficked GFP fusions.

1006

1007 To prepare the transfection mixture for one well of a 6-well plate, 5 µl of Lipofectamine-LTX and  
 1008 1000 ng of plasmid were each diluted separately into 200 µl of OptiMEM I and then combined  
 1009 and incubated at RT for 15 min, as adapted from the manufacturer's protocol. Growth media for  
 1010 each 6-well sample was replaced with 1.5 ml of OptiMEM I and the 400-µl transfection mixture  
 1011 was added dropwise to each well and incubated for 24 hours (see Cell line culture conditions).

1012 For transfections in 15-cm dishes, the transfection mixture was scaled to the number of cells  
 1013 plated.  
 1014

Lab Archive	Plasmid Description	Vector	Resistance	Purpose	Construct used in Figure(s):
pPW3403	empty (no GFP)	pEGFP	KanR	empty vector	1, 4B, 4E
pPW3404	MPZ-eGFP	pEGFP	KanR	expression of MPZ	1, 2, 4E
pPW3405	cytosolic GFP	pEGFP	KanR	expression of GFP	1C-1H
pPW3406	rhodopsin (RHO)-GFP	pRK	AmpR	expression of RHO-GFP	1 – fig sup 4 and 5, 2 –fig sup 1
pPW3407	proinsulin (INS)-GFP	pRK	AmpR	expression of INS-GFP	1 – fig sup 4 and 5
pPW3426	MPZ-ecto peptide-eGFP	pEGFP	KanR	expression of MPZ-ecto peptide (FTWRYQPEGGRDAISIFHY A)	4
pPW3427	MPZ-ecto peptide <sup>Tyr→Glu</sup> -eGFP	pEGFP	KanR	expression of MPZ-ecto <sup>Tyr→Glu</sup> peptide (FTWREQPEGGRDAISIFHE A)	4
pPW3428	MPZ-ecto peptide <sup>Arom→Glu</sup> -eGFP	pEGFP	KanR	expression of MPZ-ecto <sup>Arom→Glu</sup> peptide (ETEREQPEGGRDAISIEHE A)	4
pPW3429	DR5 long FLAG-His6x, WT with silent mutation	pRK	AmpR	expression of DR5 long isoform-FLAG, harbors silent nt mutations within signal sequence to evade siRNA (AAGACCCTTGTGCTCGTT GTC → AAaACaCTTGTGCTCGTTG TC)	4 – fig sup 1

Lab Archive	Plasmid Description	Vector	Resistance	Purpose	Construct used in Figure(s):
pPW3430	CHOP (canonical isoform)	pRK	AmpR	expression of CHOP in absence of ER stress	1 – fig sup 2

1015 **Table S1: Constructs used for protein expression in cells**

1016 **Transfections with siRNA**

1017 For experiments shown in Fig 1 and Fig S5A, the siRNA oligonucleotides against DR5 and a  
 1018 non-targeting control were purchased from Dharmacon (ON-TARGETplus Human TNFRSF10B  
 1019 8795 siRNA # L-004448-00-0005 and ON-TARGETplus Non-targeting siRNA #2 # D-001810-  
 1020 02-05). The siRNA transfection was performed as previously described in (2) using  
 1021 Lipofectamine RNAiMAX.

1022  
 1023 For the knockdown in Fig S9B, we synthesized custom siRNAs from Dharmacon siRNA  
 1024 (DR5siRNA-2: 5' AAG ACC CUU GUG CUC GUU GUC UU 3', Nt siRNA: 5' AAA CCU UGC  
 1025 CGA CGG UCU ACC UU 3'). The siRNA transfection was performed 24 hours previous to the  
 1026 DR5L-FLAG and MPZ ecto-peptide-GFP plasmid co-transfection for a knockdown of 48 h total.

1027  
 1028 **RNA extraction and generation of cDNA**

1029 Cells were grown in 6-well plates and harvested with 0.5 ml of TRIzol reagent (Life  
 1030 Technologies) per manufacturer's protocol to extract RNA. For cDNA synthesis, 500 ng of total  
 1031 RNA was reverse transcribed with 2 µl of the SuperScript VILO master mix (Life Technologies #  
 1032 11755050) in a total reaction volume of 10 µl following the manufacturer's protocol for reaction  
 1033 temperature and duration. The reverse transcription product was diluted to 200 µl with 10 mM  
 1034 Tris-HCl pH 8.2 and used at 1:100 dilution for subsequent RT-PCR reactions.

1035  
 1036 **Semi-quantitative RT-PCR for *Xbp1* mRNA splicing**

1037  
 1038 2 µl of cDNA was added to 0.2 µM of forward and reverse primers (Hs\_XBP1\_Fwd: 5' -  
 1039 GGAGTTAAGACAGCGCTTGG- 3'; Hs\_XBP1\_Rev: 5' -ACTGGGTCCAAGTTGTCCAG-3'), 0.2  
 1040 mM of each dNTP, 0.5 units of Taq DNA polymerase (Thermo Scientific). The reaction was set  
 1041 at an annealing temperature of 60.5°C with an extension time of 30 seconds for 26 cycles. The



1042 products were then visualized on a 3% agarose gel (comprised of a 1:1 mixture of low-melting  
1043 point agarose and standard agarose) stained by 1:10000 SybrSAFE.

1044  
1045 **Quantitative PCR**

1046  
1047 PCR samples were prepared as described by manufacturer's protocols from iQ SYBR Green  
1048 Supermix (BioRad #17088800).  
1049 For each experiment, qRT-PCR reactions were set up in triplicate and run using a CFX96 Real  
1050 Time System (Bio-Rad). Quantitation cycles were determined with CFX Manager 3.0 software  
1051 (Bio-Rad) and then normalized to GAPDH as an internal control.

1052  
1053

Gene	5'-forward primer-3'	5'-reverse primer-3'
MPZ	GGCCATCGTGGTTTACAC	GATGCGCTCTTTGAAGGTC
GFP	CTGACCTACGGCGTGC	CCTTGAAGAAGATGGTGCG
BiP (GRP78)	GTTTCGTGGCGCCTTGTGAC	CATCTTGCCAGCCAGTTGGG
DR5 (TNFRSF10B)	TTCTGCTTGCCTGCACCAGG	GTGCGGCACTTCCGGCACAT
CHOP (DDIT3)	AGCCAAAATCAGAGCTGGAA	TGGATCAGTCTGGAAAAGCA
GADD34	GAGGAGGCTGAAGACAGTGG	AATTGACTTCCCTGCCCTCT
GAPDH	AGCCACATCGCTCAGACAC	TGGAAGATGGTGATGGGATT

1054 **Table S2: Primers Used for Quantitative RT-PCR**

1055  
1056  
1057

**Protein analysis by Western Blot**

1058 Media and cells for each sample were collected by cell scraping into cold PBS followed by a  
1059 subsequent wash with 1 ml of cold PBS. The cell pellet was then resuspended in cold lysis  
1060 buffer (30 mM HEPES pH 7.2, 150 mM NaCl, 1% Triton X100, 1x Roche protease inhibitor) and  
1061 lysed via needle shearing on ice. Samples were centrifuged at 1000xg for 5 min, and the  
1062 supernatants were mixed with sample buffer to a final concentration of 1% SDS, 62.5 mM Tris-  
1063 HCl pH 6.8, 10% glycerol, 0.1% bromophenol blue, 50 mM DTT. Samples were boiled at 95°C  
1064 and loaded on SDS-PAGE gels (GenScript). Samples were subsequently transferred onto

1065 nitrocellulose membranes, blocked with Odyssey buffer (Licor) for 1 hour at RT, and probed with  
 1066 primary antibodies diluted 1:1000 (unless otherwise specified) in Licor Odyssey buffer  
 1067 supplemented with 0.1% Tween 20% at 4°C overnight.

Primary Antibody	Species	Catalog #
anti-DR5	rabbit	Cell Signaling Technology 8074
anti-FADD	mouse	BD Biosciences 610400
anti-GFP	mouse	Roche 11814460001
anti-PARP	rabbit	Cell Signaling Technology 9542
anti-caspase 8 5F7	mouse	MBL International M032-3
anti-caspase 3	rabbit	Cell Signaling Technology 9662
anti-GAPDH	rabbit	Abcam 9485
anti-IRE1 14C10	rabbit	Cell Signaling Technology 3294
anti-Sec31A	mouse	BD Biosciences 612350
anti-Sec23A	rabbit	Invitrogen PA5-28984
anti-RCAS1 D2B6N XP	rabbit	Cell Signaling Technology 12290
anti-Giantin	rabbit	Abcam ab24586
anti-ERGIC53	rabbit	Sigma Aldrich E1031
anti-Fc	mouse	One World Lab #603-510
anti-FLAG M2	mouse	Sigma F1804
anti-His 6x	mouse	Abcam ab15149

1068 **Table S3: Antibodies Used for Western Blots**

1069  
 1070 Bound primary antibodies were probed by HRP-conjugated secondary antibodies (Amersham,  
 1071 Piscataway, NJ, 1:10000) using enhanced chemiluminescence (SuperSignal; Thermo Scientific,  
 1072 Waltham, MA) detected by standard film or through the ChemiDoc™ XRS+ Imaging System  
 1073 (Bio-Rad).

1074  
 1075 **Caspase activity assay**

1076  
 1077 Cells harvested from a 6-well plate were resuspended in 100 µl of lysis buffer (30 mM HEPES  
 1078 pH 7.2, 150 mM NaCl, 1% Triton X-100) and lysed via needle shearing (25G, 10 passes)  
 1079 followed by a 30-min incubation on ice. Supernatant was collected after centrifuging at 1000xg  
 1080 for 5 min. For the caspase activity assay, 10 µl of supernatant diluted with lysis buffer (1:25,  
 1081 1:50, 1:100 to stay within linear range of luminescence measurements) was incubated with 10 µl  
 1082 of the luminogenic caspase glo 8 substrate (Promega #PRG8200) in a 384-white walled plate

1083 (Corning 3574) for 45 min at RT before measuring luminescence on a Spectramax-M5 plate  
1084 reader.

#### 1085 **Flow cytometry staining for apoptosis analysis**

1086  
1087 Cells seeded in a 6-well plate were transfected with the specified plasmid for 24 h and  
1088 harvested via trypsinization in complete media to allow a 30-minute recovery at 37°C. The  
1089 samples were then centrifuged at 500xg for 5 minutes and resuspended in 150 µl of a 1:20  
1090 dilution of Annexin V-AlexaFluor 647 conjugate (Thermo Scientific #A23204). Samples were  
1091 transferred to a 96-well U-bottom plate and incubated in the dark for 15 min at RT. The  
1092 distribution of apoptotic cells was determined by flow cytometry on a BD LSR II.

#### 1093 1094 **Trypan blue staining and quantification for cell death analysis**

1095  
1096 Cells seeded in a 6-well plate were transfected with the specified plasmid for 24 h and  
1097 harvested via trypsinization in complete media and ultimately resuspended in 400 µl of media to  
1098 obtain a concentration of 1.0-3.0x10<sup>6</sup> cells/ml. The cell suspension was then mixed 1:1 with  
1099 0.4% Trypan blue (Sigma-Aldrich) and incubated at 37°C for 30 min. The percentage of cells  
1100 staining positive for was then quantified using the Countess<sup>TM</sup> II FL Automated Cell Counter  
1101 (ThermoFisher, catalog # AMQAF1000) default brightfield settings with disposable slides.

1102  
1103

#### 1104 **Size-exclusion chromatography for cell lysates**

1105 Size-exclusion fractionation of cell lysate was performed as previously described in (Lu *et al.*  
1106 2014) with minor modifications.

1107 In a 15-cm dish, 4 million HCT116 cells were seeded 18 hours prior to transfection (see  
1108 Transient transfections for GFP-fusion proteins). 24 hours post-transfection, cells were  
1109 harvesting by collecting all media (to collect detached, dying cells) and scraping the dish in 3 ml  
1110 of cold PBS. The cell suspension was centrifuged at 500xg to pellet the sample. Cells were  
1111 washed with an additional 1 ml of cold PBS, pelleted, and flash frozen in liquid N<sub>2</sub> prior to lysis.

1112 Cells were resuspended in 600 µl of lysis buffer (30 mM HEPES pH 7.2, 150 mM NaCl, 1%  
1113 Triton X-100) with 1x protease inhibitor (Roche) and lysed through a 25G needle with 10  
1114 passes. Lysates were clarified by centrifugation at maximum speed for 15 min at 4°C, and the

1115 supernatant (400  $\mu$ l) was loaded onto a SuperDex200 10/300 GL column equilibrated with lysis  
1116 buffer at a flow rate of 0.35 ml/min. Fractions were collected in 0.5 ml aliquots.

1117 For the caspase 8 activity assay, 10  $\mu$ l of each fraction was incubated with 10  $\mu$ l of the caspase  
1118 glo 8 substrate (Promega #PRG8200) in a 384-well white walled plate (Corning 3574) for 45 min  
1119 at RT before measuring luminescence on a Spectramax-M5 plate reader.

1120 For Western blots, every three fractions were pooled for a total of 1.5 ml and subjected to TCA  
1121 precipitation to concentrate the protein content. Samples were then analyzed by SDS-PAGE  
1122 and immunoblotted for GFP and DR5.

### 1123 **DR5 Immunoprecipitation (IP)**

1124  
1125 IP for DR5 was performed as previously described in (Lu *et al.* 2014), using anti-DR5 mAb 5C7-  
1126 conjugated agarose beads gifted by David Lawrence of the Ashkenazi lab at Genentech Inc.

### 1127 1128 **GFP Immunoprecipitation (IP)**

1129  
1130 15-cm dishes were seeded with 4 million HCT116 cells and allowed to recover for 18 hours prior  
1131 to transfection. Samples were then transfected for 24 hours with the GFP-tagged ER trafficked  
1132 protein, cytosolic GFP, or empty vector. To harvest apoptotic and living cells for each sample,  
1133 all media and washes were collected. Cells were scraped in 2 ml of cold PBS and combined  
1134 with the media and washes. Samples were centrifuged to pellet cells, washed with 1 ml cold  
1135 PBS, and flash frozen in liquid N<sub>2</sub> prior to lysis.

1136  
1137 The cell pellets were resuspended in 750  $\mu$ l of 30 mM HEPES pH 7.2, 150 mM NaCl, 1% Triton  
1138 X-100 with 1x Roche protease inhibitor cocktail (if used subsequently for caspase glo 8 assay)  
1139 or with 5x Roche protease inhibitor cocktail (if used for immunoblotting). The cells were lysed by  
1140 mechanical shearing through a 25G needle for 13-15 plunges followed by incubation on ice for  
1141 30 min. The lysate was centrifuged at 2000xg for 5 min to remove debris and then incubated  
1142 with 30  $\mu$ l of GFP-Trap magnetic agarose beads (Chromotek gtma-20) for 4 hours at 4°C. The  
1143 beads were then washed with 750  $\mu$ l of lysis buffer for 10 min at 4°C for three rounds.

1144  
1145 For measuring caspase activity, a fifth of the beads was resuspended in 40  $\mu$ l of 30 mM HEPES  
1146 pH 7.2, 150 mM NaCl, 1% Triton X-100. 10  $\mu$ l of the resuspended mixture was incubated with

1147 10  $\mu$ l of the caspase glo 8 luminogenic substrate (Promega #PRG8200) for 45 min at RT before  
1148 measuring luminescence.

1149  
1150 For Western blots, samples were eluted by adding 35  $\mu$ l of non-reducing SDS gel loading buffer  
1151 (50 mM Tris-HCl (pH 6.8), 2% SDS, 0.1% bromophenol blue, 10% glycerol) and incubated for  
1152 10 min at 70°C. The beads were then magnetically removed from the eluted sample before  
1153 adding DTT to a final concentration of 25 mM. The entire sample was loaded onto the gel and  
1154 immunoblotted for DR5, caspase 8, and GFP, in that order.

1155  
1156 **Immunofluorescence of DR5 and organelle markers in HCT116**

1157  
1158 HCT116 were seeded at 25000 cells per well in an eight-well glass-bottom  $\mu$ Slide (Ibidi 80827)  
1159 pre-coated with Collagen IV (Sigma-Aldrich C6745, 0.03 mg/ml in PBS incubated for 30 min at  
1160 RT, and then rinsed off with PBS x 3) in growth media 18 hours prior to transfection (see above  
1161 for protocol). 24 hours post-transfection, the cells were fixed using 4% paraformaldehyde (PFA,  
1162 Electron Microscopy Sciences) or methanol, depending on the antibody combination used for  
1163 immunostaining (see table below). Samples were protected from light after fixation to preserve  
1164 GFP fluorescence.

1165  
1166

Primary Antibody	Species	Catalog #	IF Dilution	Fixation method
anti-DR5 3H3	mouse	Genentech	1:100	4% PFA/methanol
anti-cleaved caspase 8 (Asp391) (18C8)	rabbit	Cell Signaling Technology 9496	1:50	4% PFA
anti-RCAS1 D2B6N XP	rabbit	Cell Signaling Technology 12290	1:200	methanol
anti-Giantin	rabbit	Abcam ab24586	1:1000	methanol
anti-ERGIC53	rabbit	Sigma Aldrich E1031	1:100	methanol

1167 **Table S4: Antibodies Used for Immunofluorescence**

1168  
1169 For fixation with 4% PFA, 32% PFA was added directly to the well in growth media for a 1:8  
1170 dilution and incubated for 10-15 min at RT. Cells were then permeabilized with PHEM buffer  
1171 (60 mM PIPES, 25 mM HEPES, 10 mM EGTA, 2 mM MgCl<sub>2</sub>-hexahydrate, pH 6.9) containing  
1172 0.1% Triton-X100 for 10 min at RT for three washes.

1173  
1174 For fixation with methanol, media was removed and cells were washed with cold PBS. Then  
1175 methanol (pre-cooled at -20°C) was added to the well and incubated at -20°C for 3-4 min. The  
1176 methanol was promptly aspirated and replaced with PHEM buffer (without Triton X-100),  
1177 followed by two more 10-min washes with PHEM at RT.

1178  
1179 To block against non-specific antibody interactions, cells were rinsed in PHEM (without 0.1%  
1180 Triton X-100) and then incubated with PHEM containing 2% normal goat serum (Jackson  
1181 Immunoresearch Laboratories, 005-000-121) for 1 hr at RT. Primary antibodies were incubated  
1182 in blocking solution overnight at 4°C at the dilution noted in the table above. Cells were then  
1183 washed with PHEM buffer for 10 min at RT x 3 and incubated with secondary antibodies, anti-  
1184 mouse-AlexaFluor546 (Invitrogen A11030) and anti-rabbit-AlexaFluor633 (Invitrogen A21071),  
1185 diluted 1:1000 in PHEM with 2% normal goat serum. (Secondary antibody solutions were  
1186 centrifuged at 15000xg for 20 mins at 4°C to remove aggregates prior to incubating with cell  
1187 samples.) After a 1-hr incubation at RT, cells were washed with PHEM buffer once, then  
1188 incubated with PHEM buffer containing nuclear stain (DAPI, Molecular Probes, Eugene, OR, D-  
1189 1306, 5 µg/mL), and finally rinsed with PHEM buffer twice before imaging.

1190  
1191 Samples were imaged on a spinning disk confocal with Yokogawa CSUX A1 scan head, Andor  
1192 iXon EMCCD camera, and 40x Plan Apo air Objective NA 0.95 or 100x ApoTIRF objective NA  
1193 1.49 (Nikon).

1194  
1195 **Quantification of Pearson's correlation for co-localization analyses**

1196  
1197 Images were analyzed using CellProfiler (Carpenter *et al.* 2006). From the 405 nm channel, cell  
1198 nuclei were identified as primary objects using maximum correlation thresholding (MCT) and  
1199 shape to distinguish clumped objects. Secondary objects were outlined using propagation from  
1200 the nuclei (DAPI) after applying MCT from the 488 nm, 561 nm, and 633 nm channels. Tertiary  
1201 objects for each cell was identified as the mask of each nucleus subtracted from the mask of its  
1202 corresponding secondary object in each channel, yielding masks for intracellular GFP-tagged

1203 protein from the 488 nm channel, for intracellular DR5 from the 561 nm channel, and for the  
1204 organelle marker in the 633 nm channel. For overlap between DR5 and MPZ/RHO-GFP,  
1205 Pearson's correlation coefficients were calculated within the MPZ/RHO mask for each cell to  
1206 filter out untransfected cells. For overlap between DR5/MPZ and organelle markers, Pearson's  
1207 correlation coefficients were calculated within tertiary objects for the organelle marker in GFP+  
1208 cells. Statistical analyses for all data sets were performed using GraphPad Prism 6.0.

1209

### 1210 **Subcellular fractionation**

1211

1212 This subcellular fractionation protocol was adapted from (Xu *et al.* 2015).

1213

1214 Cells transfected with MPZ-GFP were harvested from a 15-cm dish as described in the Size  
1215 Exclusion Chromatography section above. The cell pellet was resuspended in 400  $\mu$ l of  
1216 homogenization buffer (10 mM triethanolamine-acetic acid, pH 7.4, 0.25 M sucrose, 1 mM  
1217 sodium EDTA, protease inhibitor cocktail (Roche)) and lysed via mechanical shearing  
1218 through a 25-gauge needle on a 1-ml syringe with 13 passes. (Note on protease inhibitor: 4x  
1219 protease inhibitor was used to lyse samples used for Western blotting to minimize  
1220 degradation of proteins, while 1x protease inhibitor was used in sample lysis for caspase glo  
1221 8 assay so that excess inhibitor would not interfere with cleavage of luminescent substrate.)  
1222 Homogenized sample was then centrifuged at 2000xg for 15 min at 4°C to remove unlysed  
1223 cells and the nuclear fraction. 250  $\mu$ l of the supernatant was loaded via capillary action onto a  
1224 9-25% iodixanol gradient in a 13x51mm polyclear centrifuge tube (Seton Scientific # 7022-  
1225 29426) prepared using the BioComp Gradient Master (Model 107). The 9% and 25% layers of  
1226 the gradient were made by diluting 60% iodixanol (OptiPrep<sup>TM</sup> Density Medium, Sigma Aldrich #  
1227 D1556) into cell suspension medium (0.85% (w/v) NaCl, 10 mM Tricine-NaOH, pH 7.4). The  
1228 loaded gradients were then centrifuged in SW55Ti rotor at 44800 rpm for 2 hr at 4°C. After  
1229 deceleration without braking, 300- $\mu$ l fractions were collected from the top of the tube.

1230

1231 Fractions from samples lysed with 4x protease inhibitor were subjected to TCA precipitation to  
1232 concentrate protein content for immunoblotting. Fractions from samples lysed with 1x protease  
1233 inhibitor were used for the caspase glo 8 assay (10  $\mu$ l of each fraction + 10  $\mu$ l of the caspase glo  
1234 8 reagent (Promega #PRG8200) incubated for 45 min at RT prior to measuring luminescence).

1235

### 1236 **Peptide Array Binding**

1237

1238 Peptide arrays were purchased from the MIT Biopolymers Laboratory as described previously in  
 1239 (Karagöz *et al.* 2017) and (Gardner and Walter 2011). The sequences of each protein were tiled  
 1240 from N- to C-terminus in 18-amino-acid-long peptides shifting by three amino acids from the  
 1241 previous spot. The arrays were incubated in methanol for 10 min, and then washed in binding  
 1242 buffer (50 mM HEPES pH 7.2, 250 mM NaCl, 10% glycerol) for 10 min at room temperature x 3.  
 1243 500 nM of Fc-tagged DR5 extracellular domain (ECD, a kind gift from Scot Marsters) was  
 1244 incubated with the array in binding buffer at room temperature for 1 hr. Then, the array was  
 1245 washed three times for 10 minutes with binding buffer to remove unbound protein. The bound  
 1246 DR5 ECD was then transferred onto a nitrocellulose membrane via a semi-dry transfer  
 1247 apparatus (Owl HEP-1) at 80 mA for 45 min at 4°C. The membrane was then blocked with  
 1248 1xPBST with 5% milk for 1 hr at room temperature and probed with 1:1000 anti-Fc (One World  
 1249 Lab #603-510) overnight at 4°C followed by 1:10000 anti-mouse IgG-HRP (Promega #W4021)  
 1250 for 1 hr at RT. The membrane was imaged using chemi-luminescence with the Bio-Rad  
 1251 Universal Hood II Gel Doc below saturating pixel intensities. The signal of each spot was  
 1252 quantified using Max Quant and normalized to the maximum intensity of all the spots on the  
 1253 same array.

#### 1254 **Peptides**

1255 Peptides were ordered from GenScript at >95% purity and stored with desiccant at -20°C.  
 1256 Peptides were dissolved as a highly concentrated stock solution in anhydrous DMSO and  
 1257 diluted 1:50 in aqueous buffer to measure the stock concentration using absorbance at 280 nm.  
 1258 All solution mixtures containing peptide and protein had a final concentration of 0.5% DMSO.  
 1259

peptide	peptide sequence
MPZ-ecto <sup>VD</sup>	VSDDISFTWRYQPEGGRD
MPZ-ecto	FTWRYQPEGGRDAISIFHYA
MPZ-ecto <sup>Tyr→Glu</sup>	FTWREQPEGGRDAISIFHEA

**Table S5: Amino Acid Sequences of MPZ-derived Peptides**

1260  
1261

#### 1262 **Peptide pulldown with Fc-tagged ECD proteins**

1263 Recombinant Fc-tagged DR5 and TNFR1 ECD proteins were generated and purified at  
 1264 Genentech Inc by S. Marsters.

1265 Fc-tagged proteins were incubated with Dynabeads Protein G (20 µg per 12.5 µl of beads for



1266 each sample) in 1xPBS for 1.5 hours at RT. Beads were then washed with 1xPBS via magnetic  
 1267 pulldown, followed by two 10-min washes with 20 mM HEPES pH 7.2, 100 mM KOAc, 0.2%  
 1268 Tween-20 at RT to remove unbound Fc-tagged protein. Protein bound-beads were incubated  
 1269 with 50  $\mu$ l of 100  $\mu$ M peptide in 20 mM HEPES pH 7.2, 100 mM KOAc, 0.2% Tween-20 for 1  
 1270 hour at RT. Beads were then washed with 50  $\mu$ l of buffer three times, and samples were eluted  
 1271 with 25  $\mu$ l of non-reducing sample buffer (62.5 mM Tris-HCl pH 6.8, 2.5% SDS, 10% glycerol)  
 1272 by incubating at 65°C for 15 min to elute the complex.

### 1273 **Purification of recombinant of DR5 and TNFR1 ECD**

1274 Human DR5 ECD (long isoform, residues 72-213:  
 1275 KRSSPSEGLCPPGHHISEDGRDCISCKYGGDYSTHWNDLLFCLRCTRCDSDGEVELSPCTTTRN  
 1276 TVCQCEEFTFREEDSPEMCRKCRGTGCPRGMVKVGDCPTWSDIECVHKESGTKHSGEVPAVE  
 1277 ETVTSSPGTPASPCSLSG) and TNFR1 ECD (residues 22-211:  
 1278 IYPSGVIGLVPHLGDREKRDSVCPQGKYIHPQNNNSICCTKCHKGTLYNDPCGPGQDTCRE  
 1279 ESGSFTASENHLRHCLSCSKCRKEMGQVEISSCTVDRDTCGCRKNQYRHYWSENLFQCFN  
 1280 CSLCLNGTVHLSCQEKQNTVCTCHAGFFLRENECVSCSNCKKSLECTKLCLPQIENVKGTEDS  
 1281 GTT) were cloned into a pFastBac HTB vector containing a Gp67 (glycoprotein) signal peptide  
 1282 and 6xHis tag to force secretion of the expressed protein. The pFastBac HTB constructs were  
 1283 recombined into bacmid DNA using the Bac-to-Bac baculovirus expression system according to  
 1284 manufacturer's protocols (Life Technologies).

Lab Archive	Plasmid Description	Vector	resistance	Construct used in Figure(s):
pPW3408	Gp64-His6x-DR5 long ECD-FLAG	pFastBacHT	AmpR	3D-3F
pPW3410	Gp64-His6x-DR5 long ECD	pFastBacHT	AmpR	3C
pPW3411	Gp64-His6x-TNFR1 ECD	pFastBacHT	AmpR	3C

1285 **Table S6: Constructs used to generate bacmid for recombinant protein purification**

1286 SF21 were grown in SF-900 II media supplemented with 10% FBS at 28°C in disposable  
 1287 Erlenmeyer flasks rotating at 150 rpm and transfected using Cellfectin II (Thermo Fisher  
 1288 Scientific) according to manufacturer's protocols. The baculovirus was amplified two more times

1289 at a low M.O.I. prior to infection of SF21 with a 1:50 dilution of the virus for protein expression.

1290 After 72-96 hr of infection, the SF21 suspension was centrifuged at 2000xg for 15 min (two  
 1291 rounds) to collect the media containing the secreted ECD protein. The media was then further  
 1292 clarified through a 0.2  $\mu$ m filter before loading onto a HisTrapFF column equilibrated with 25 mM  
 1293 imidazole pH 7.4, 150 mM NaCl (Buffer A) at a flow rate of 3.0 ml/min. The column was washed  
 1294 with 20 CV of Buffer A at a flow rate of 4.0 ml/min. To elute, the concentration of imidazole was  
 1295 increased through a linear gradient from 0-100% of Buffer B (500 mM imidazole pH 7.4, 150  
 1296 mM NaCl) in 7 CV. Fractions containing the His-tagged ECD were then concentrated and  
 1297 further purified on a SuperDex200 10/300 GL column (GE Healthcare) equilibrated with 30 mM  
 1298 HEPES pH 7.2, 150 mM NaCl. For long-term storage, the protein was diluted into 30 mM  
 1299 HEPES pH 7.2, 150 mM NaCl, 10% glycerol and flash frozen in liquid N<sub>2</sub> before storing at -  
 1300 80°C.

#### 1301 **Labeling of DR5 and TNFR1 ECD**

1302 Recombinant DR5 and TNFR1 ECD were labeled with AlexaFluor647 NHS Ester (Succinimidyl  
 1303 Ester) (Life Technologies # A37573) in a 3:1 dye:protein molar ratio in 30 mM HEPES pH 7.2,  
 1304 150 mM NaCl, 1% DMF overnight at 4°C protected from light. The labeled proteins were re-  
 1305 loaded onto a SuperDex200 10/300 GL column to remove the excess dye, yielding labeling  
 1306 efficiencies of 59% and 49% for DR5 ECD and TNFR1 ECD, respectively. Labeled proteins  
 1307 were diluted into buffer with 10% glycerol and flash frozen in liquid N<sub>2</sub> for long-term storage at -  
 1308 80°C.

#### 1309 **Fluorescence quenching assay**

1310 To set up reactions, the unlabeled peptide titration (10  $\mu$ l each) was made from a two-fold  
 1311 dilution series of the highest peptide concentration assayed. To each peptide sample, 10  $\mu$ l of  
 1312 AlexaFluor647-labeled ECD protein was added to give a final concentration of 200 nM ECD  
 1313 protein in 20 mM HEPES pH 7.2, 100 mM KOAc, 0.1% Tween-20. Samples were incubated for  
 1314 30 min at RT protected from light before measuring fluorescence.

1315 Samples were then loaded by capillary action onto premium capillaries (NanoTemper  
 1316 Technologies, cat. #MO-K025). Fluorescence was measured on a Monolith NT.115 Instrument  
 1317 (NanoTemper Technologies, Germany) using the capillary scan function at 25°C.  
 1318 The half-maximum binding constant ( $K_{1/2}$ ) and Hill coefficient were determined by fitting the data  
 1319 points on Prism 6.0 to the model equation:  $Y=B_{\max} * X^h / (K_{1/2}^h + X^h)$ , where Y is the %

1320 quenching,  $X$  is the concentration of peptide,  $B_{\max}$  is the maximum % quenching, and  $h$  is the  
1321 Hill slope.

1322

### 1323 **Crosslinking for DR5 ECD and peptide**

1324

1325 To set up the peptide titration series, two-fold dilutions were made from the highest peptide  
1326 concentration used into 20 mM HEPES pH 7.2, 150 mM NaCl. An equal volume of C-terminal  
1327 FLAG-tagged DR5 ECD was added to each peptide sample or buffer alone for a final  
1328 concentration of 10  $\mu$ M DR5 ECD. Reactions were equilibrated at RT for 30 min prior to the  
1329 addition of 100  $\mu$ M BS3 for 20 min at RT. Excess crosslinker was quenched by adding Tris-HCl  
1330 pH 7.4 to a final concentration of 100 mM and incubated for 15 min at RT before analysis by  
1331 SDS-PAGE. The resulting gel was then transferred onto a nitrocellulose membrane (120 V, 2  
1332 hours for high MW species) and blotted with anti-FLAG to visualize discrete crosslinked species.

1333

### 1334 **Size exclusion of DR5 ECD and peptide complex**

1335

1336 The specified concentration of protein and peptide were incubated overnight at 4°C. The  
1337 following day, 200  $\mu$ l of each sample was loaded onto a SuperDex200 10/300 GL column  
1338 equilibrated with 30 mM HEPES pH 7.2, 150 mM NaCl at a flow rate of 0.5 ml/min. Fractions  
1339 were collected in 1-ml aliquots.

1340 For subsequent analysis of each fraction by SDS-PAGE, 1-ml fractions were concentrated to 50  
1341  $\mu$ l using a 3kDa MW cutoff and loaded onto a gel. The fluorescein-labeled peptide was  
1342 visualized using the fluorescence detection mode on a Typhoon 9400 Variable Mode Imager  
1343 (GE Healthcare). Protein was visualized by staining with Coomassie.

Figure 1

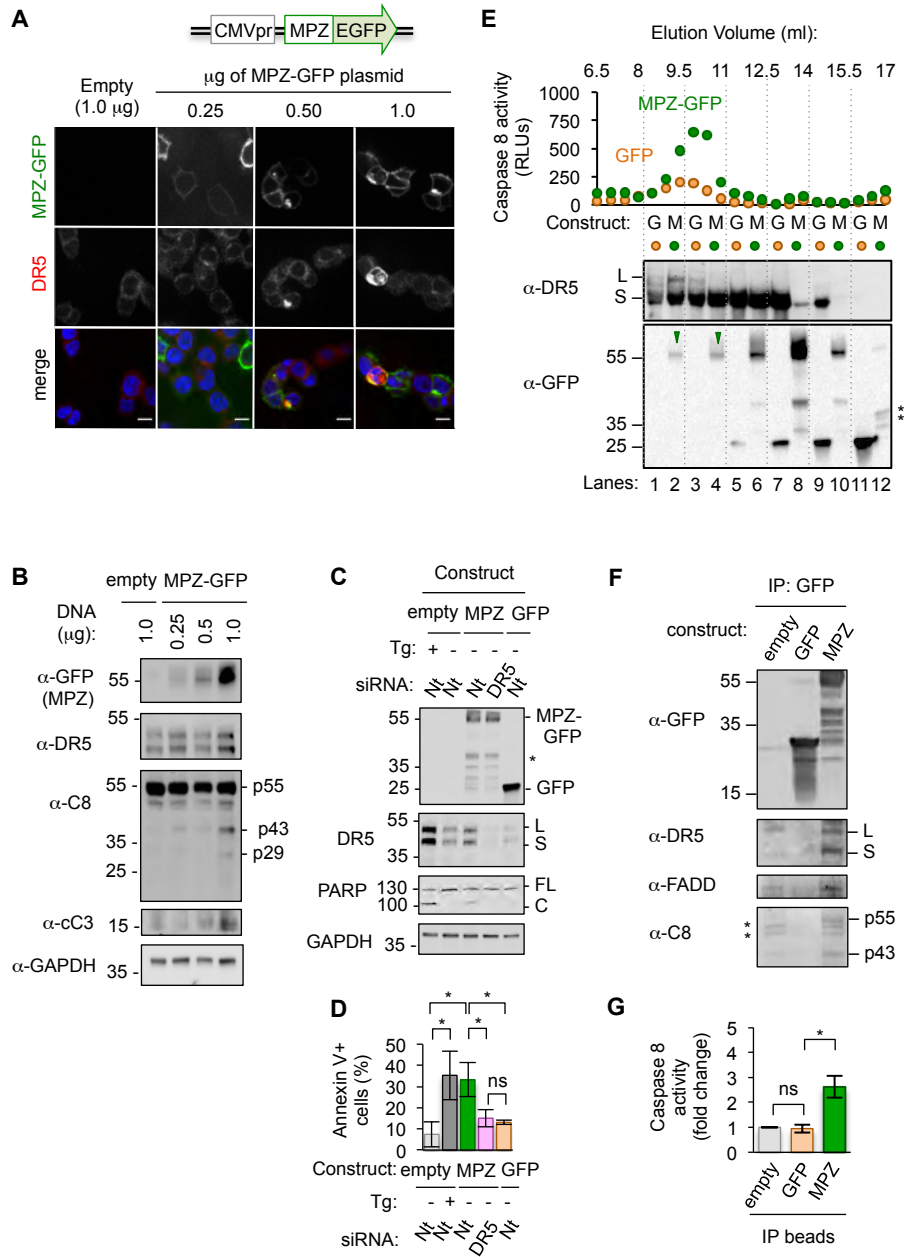


Figure 1–figure supplement 1

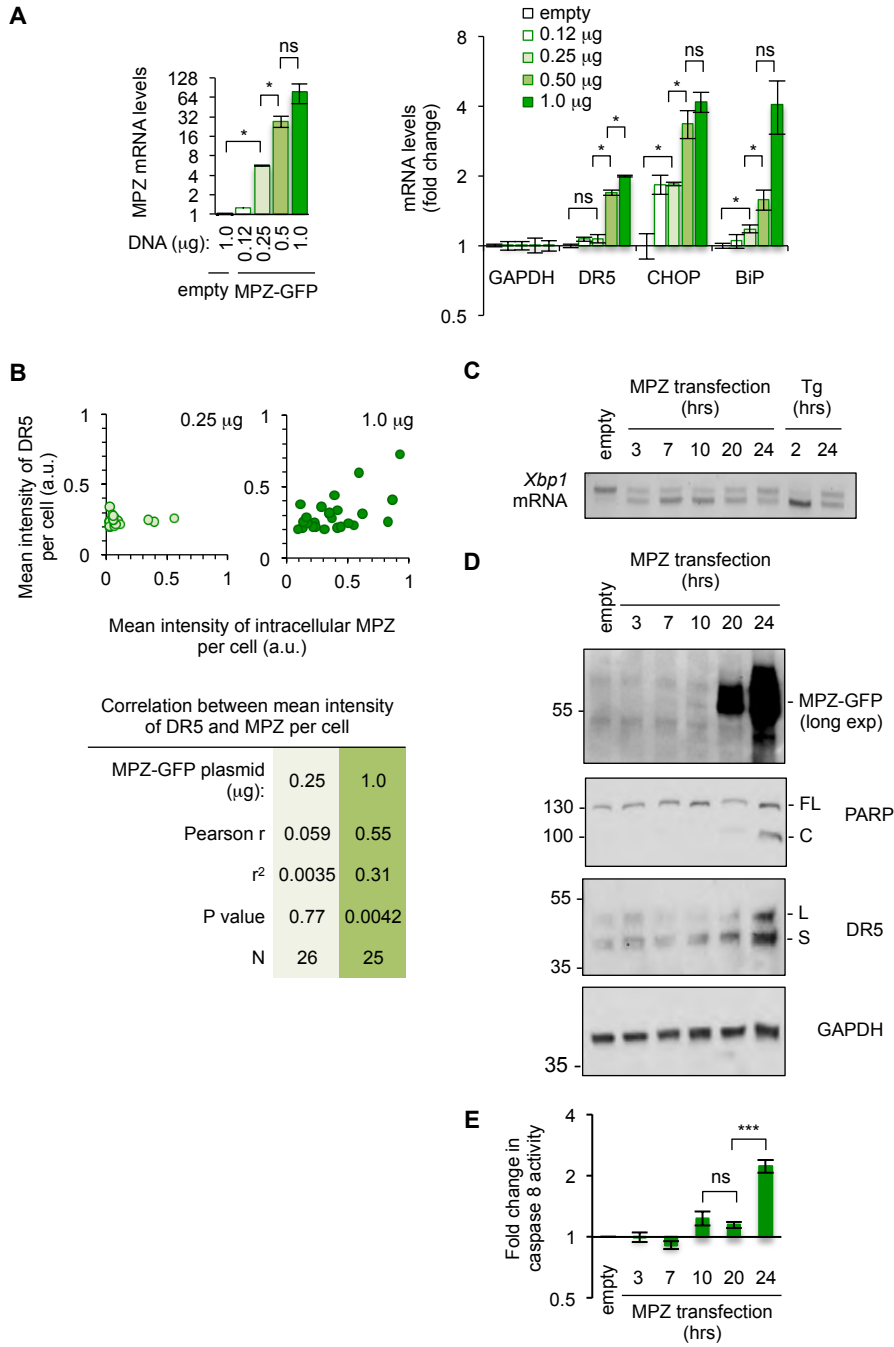


Figure 1–figure supplement 2

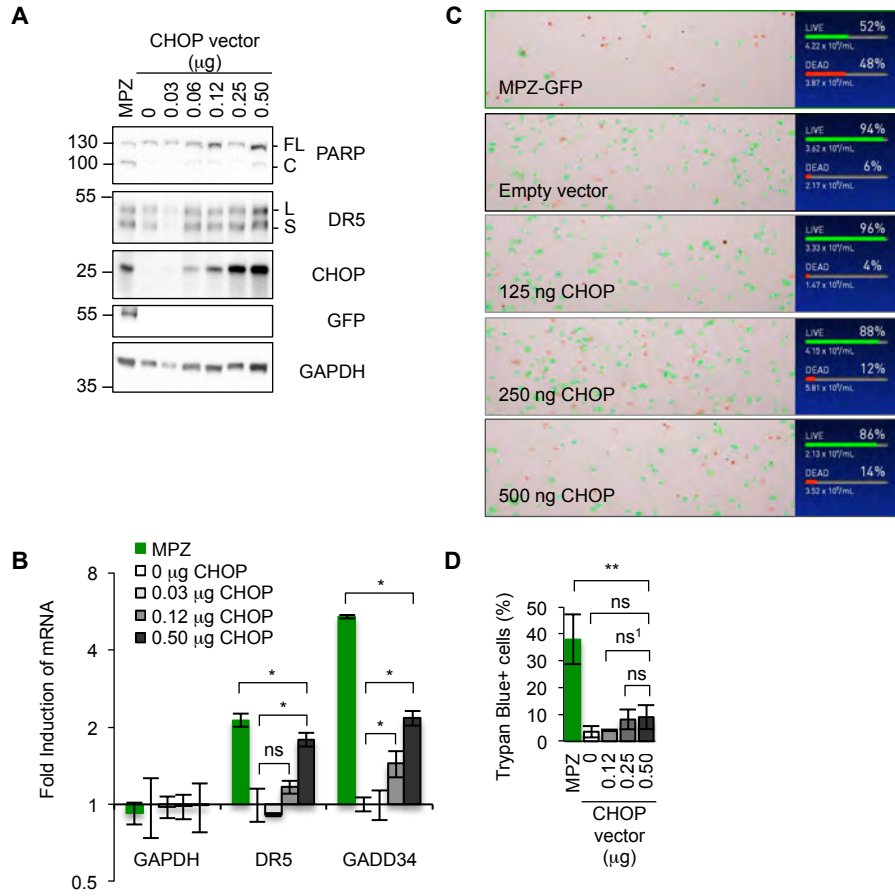
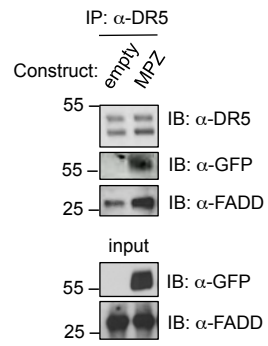
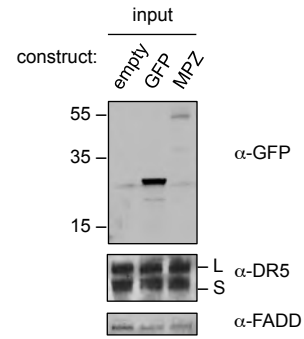


Figure 1–figure supplement 3

**A**



**B**



**C**

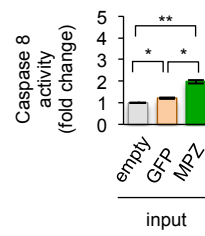


Figure 1–figure supplement 4

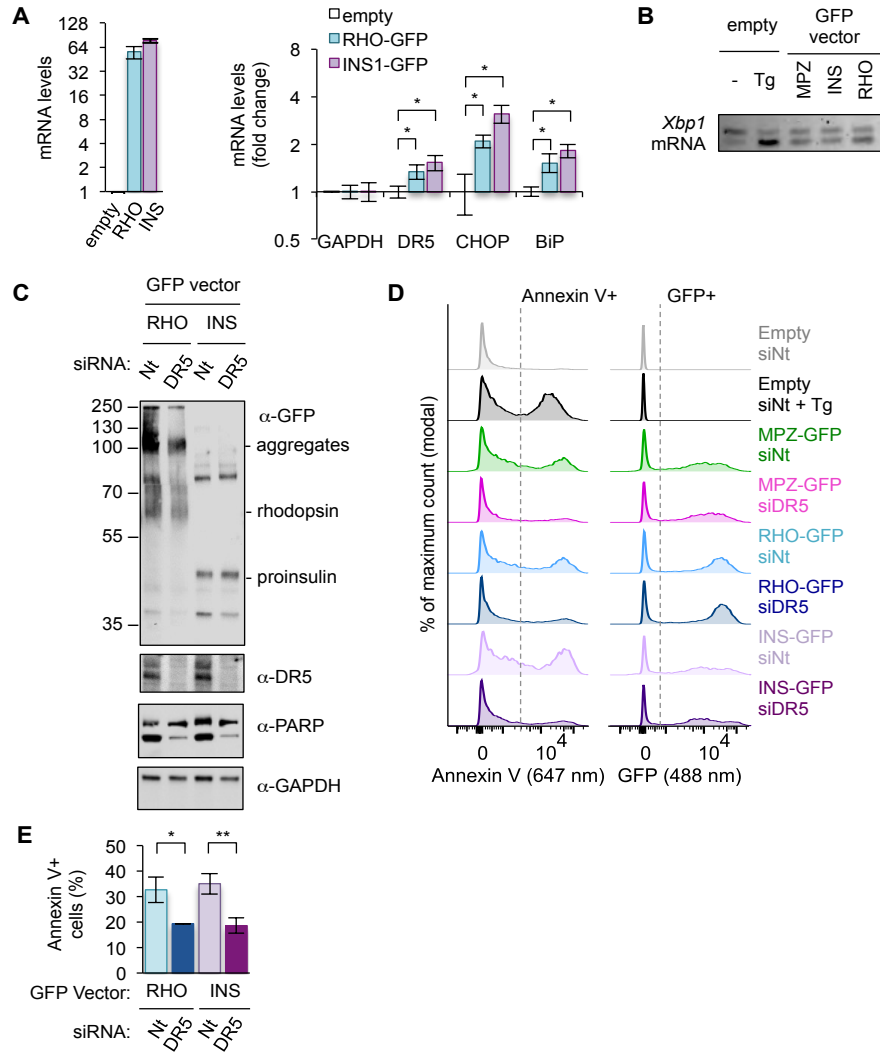




Figure 1–figure supplement 5

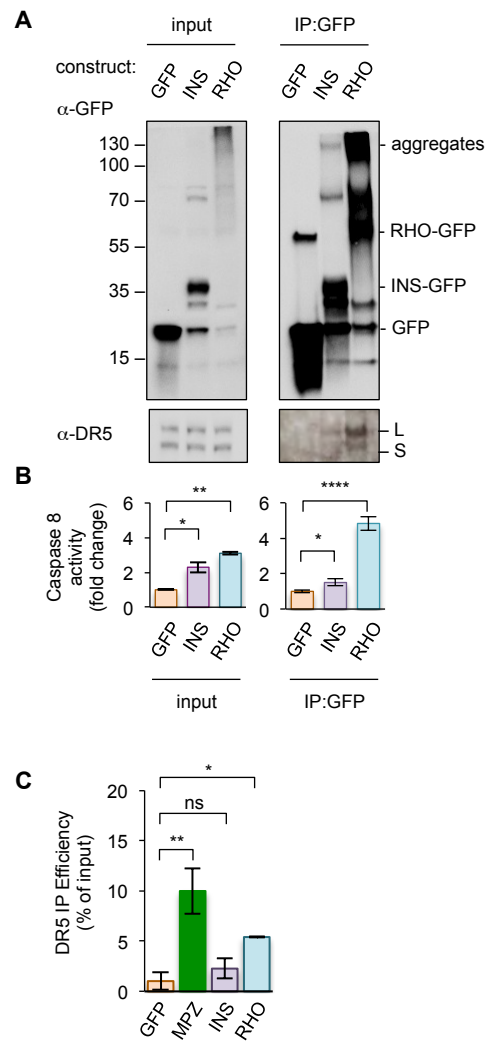


Figure 2

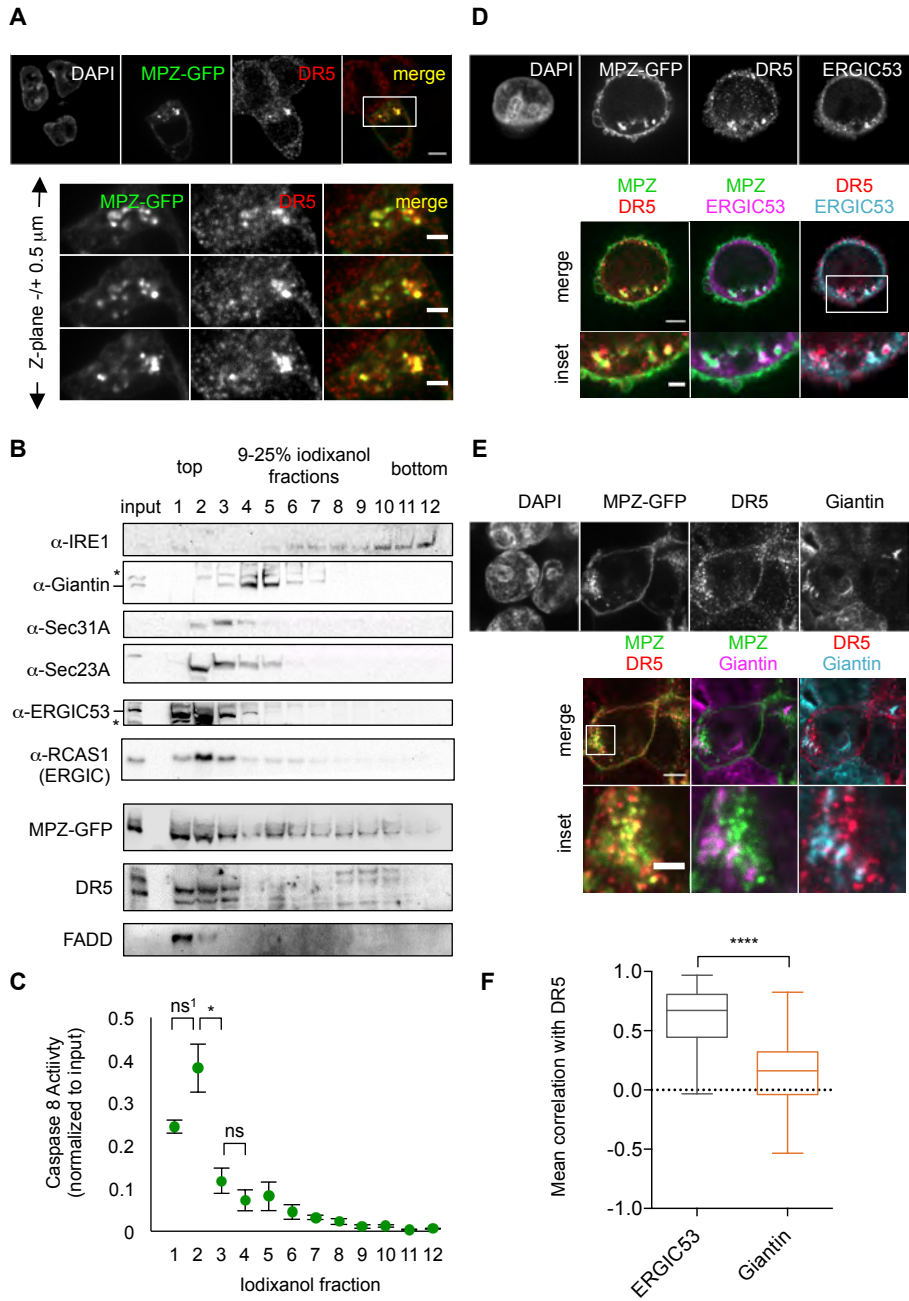


Figure 2–figure supplement 1

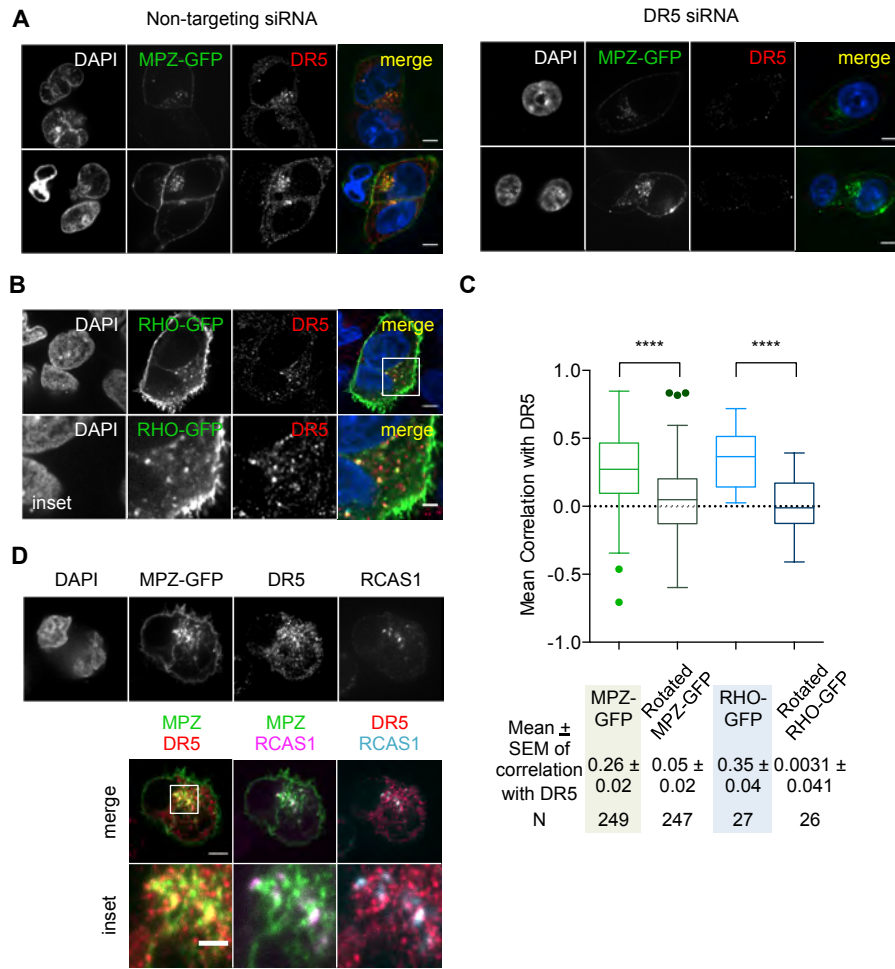


Figure 2–figure supplement 2

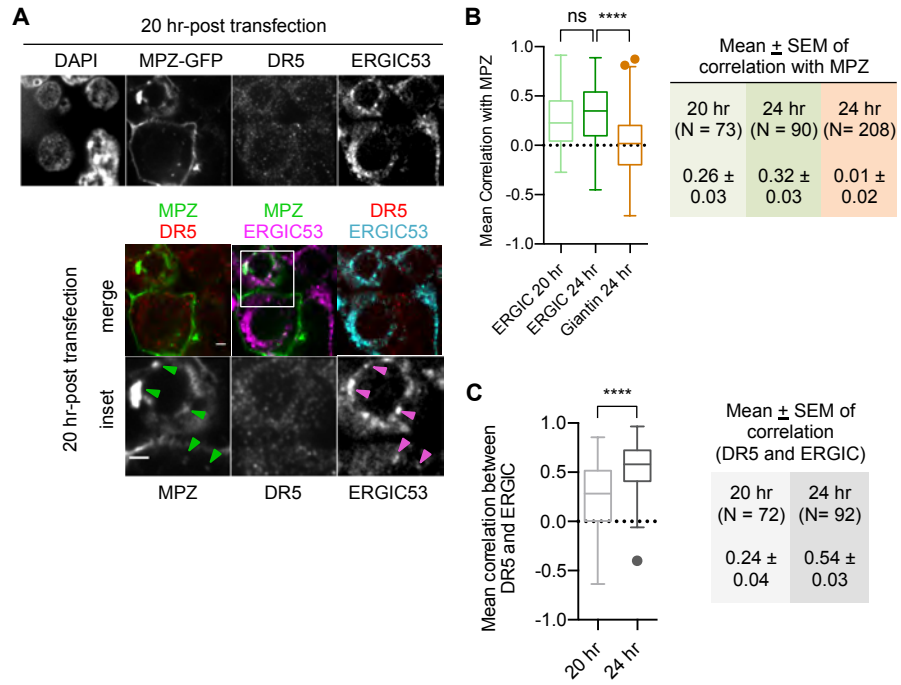


Figure 3

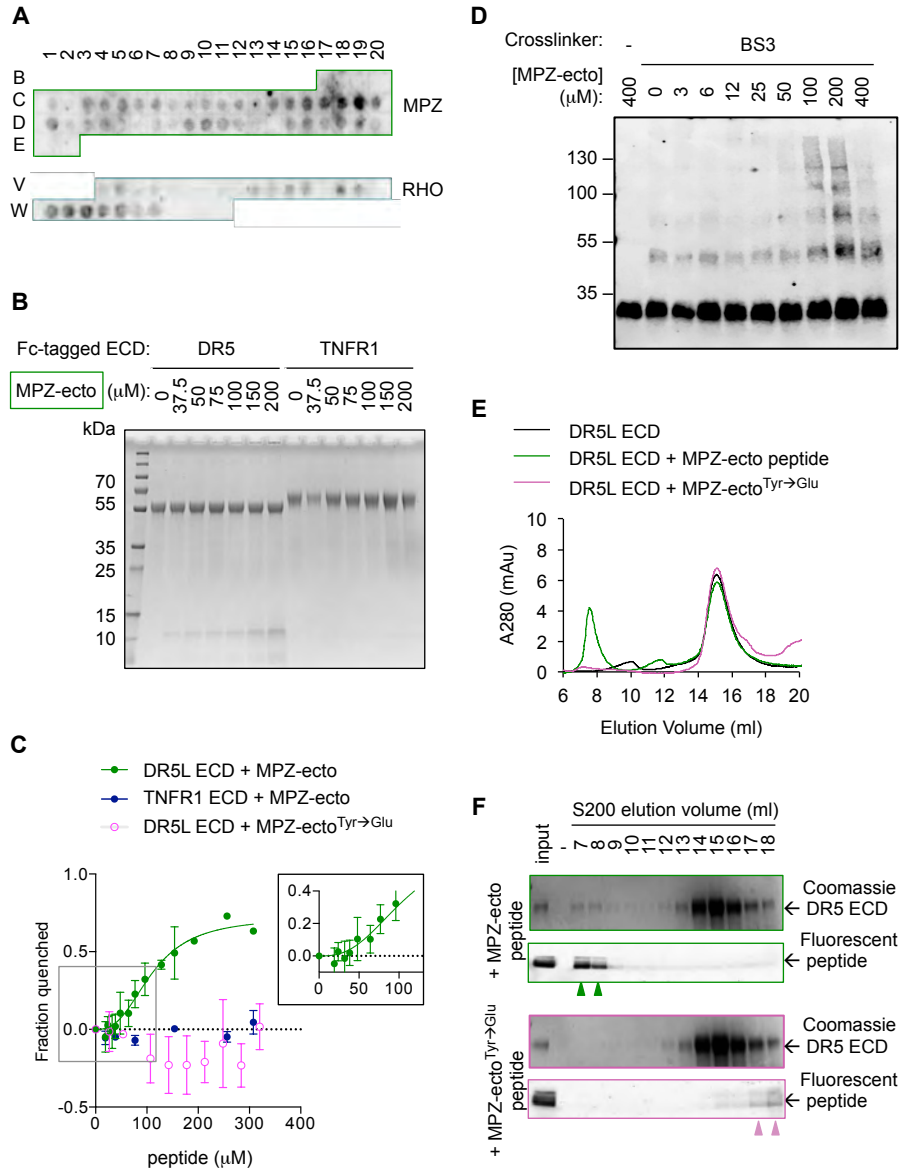


Figure 3–figure supplement 1

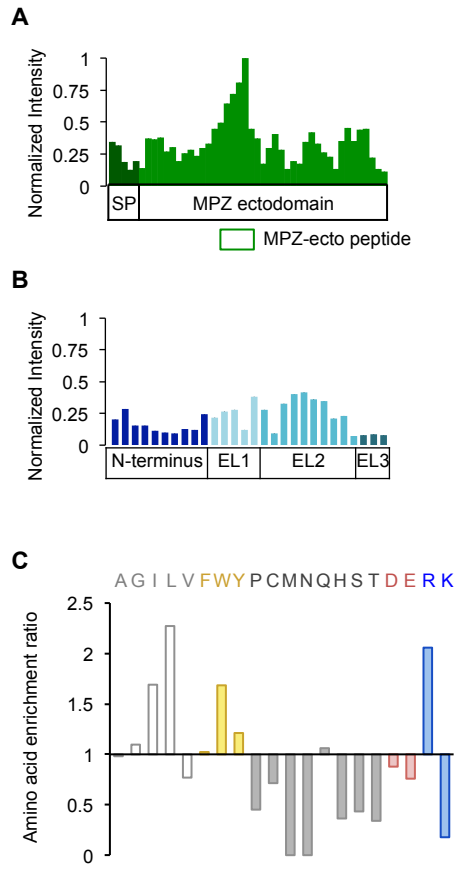


Figure 3—figure supplement 2

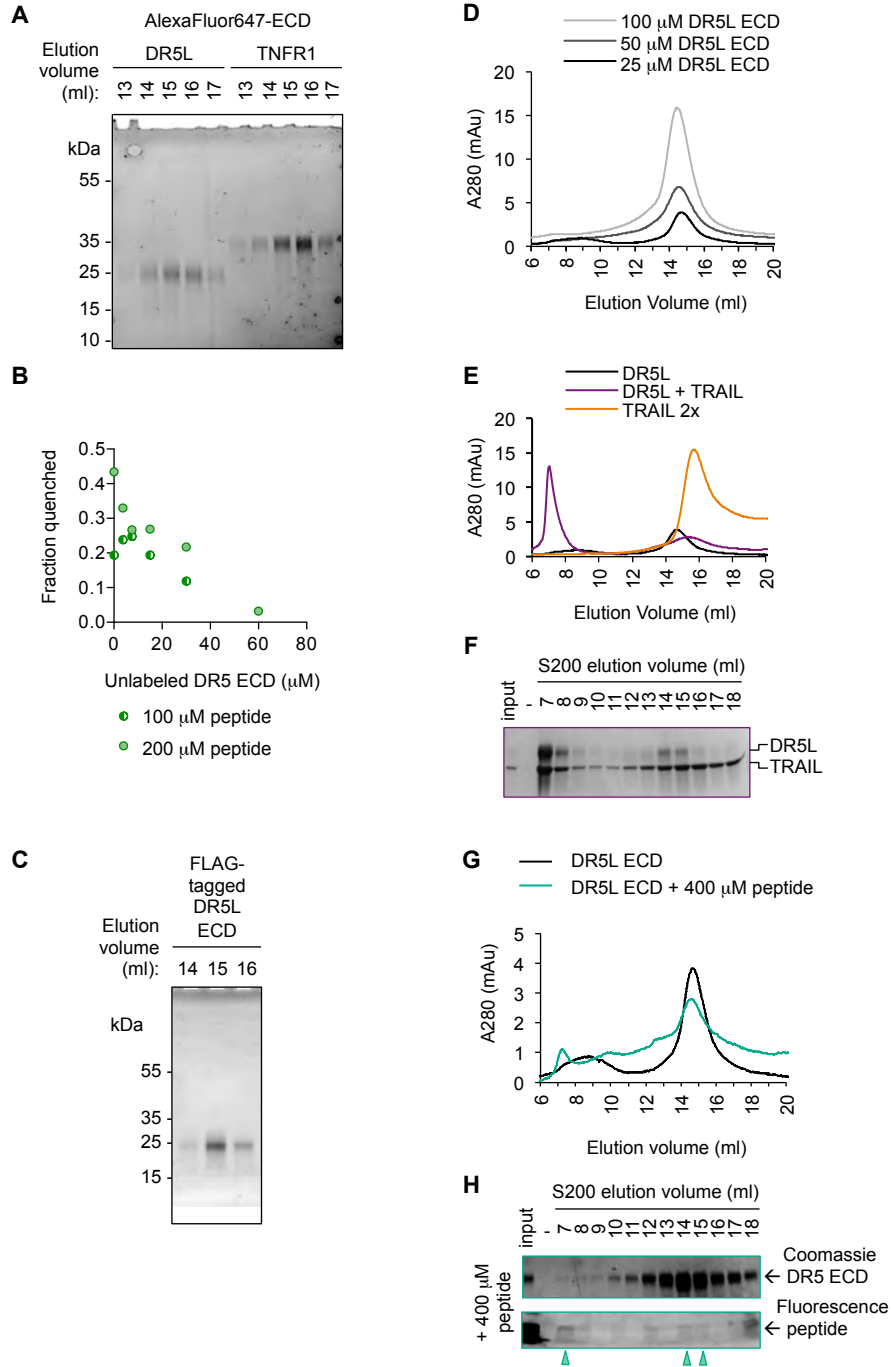


Figure 4

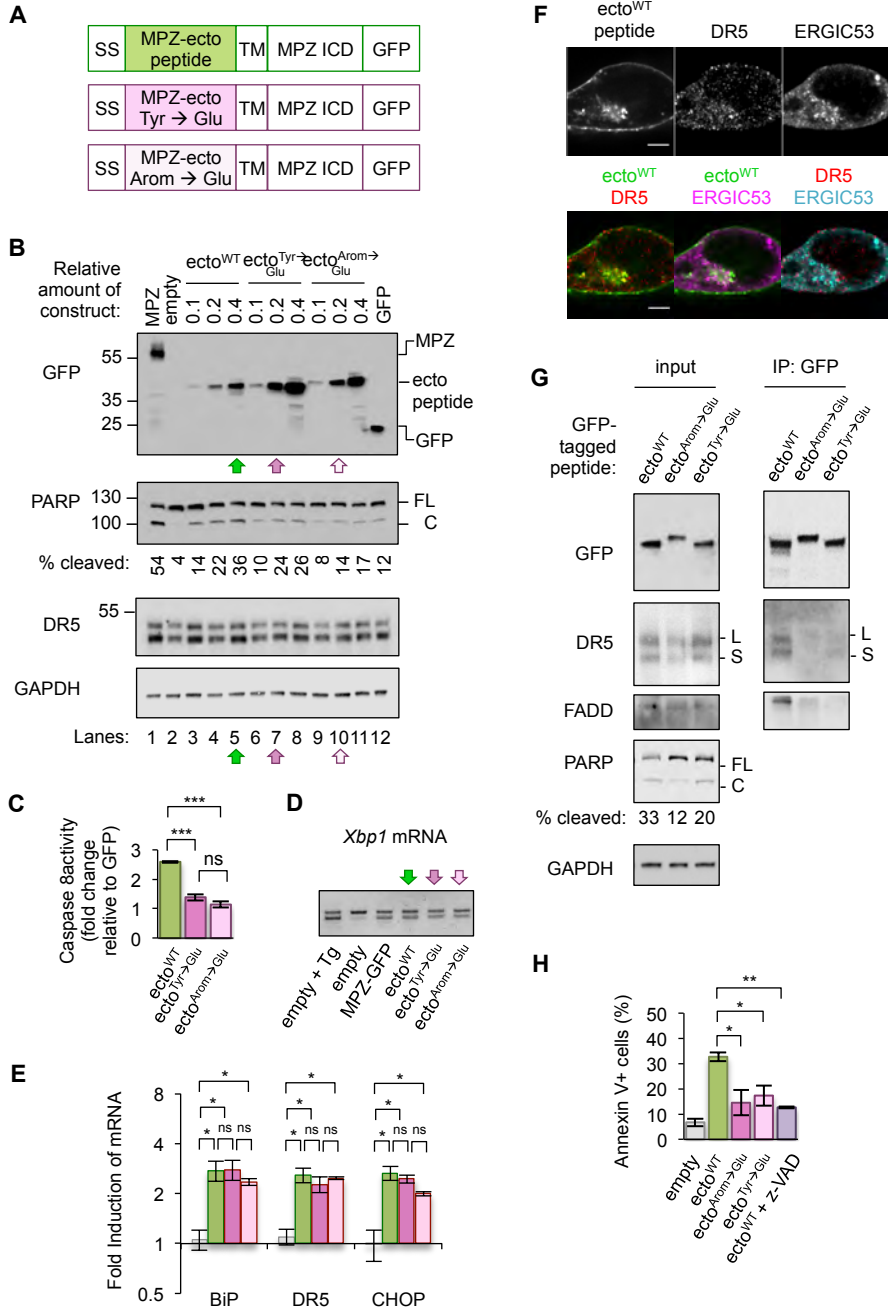




Figure 4-figure supplement 1

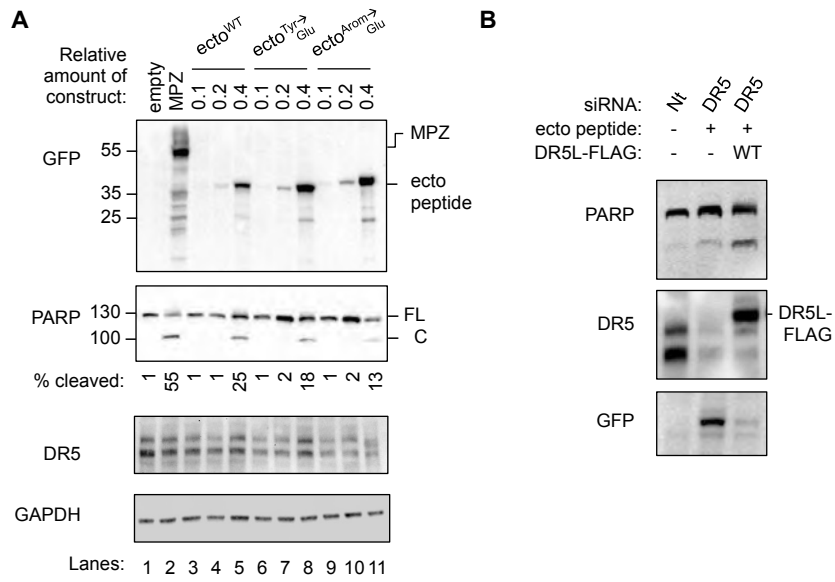


Figure 4–figure supplement 2

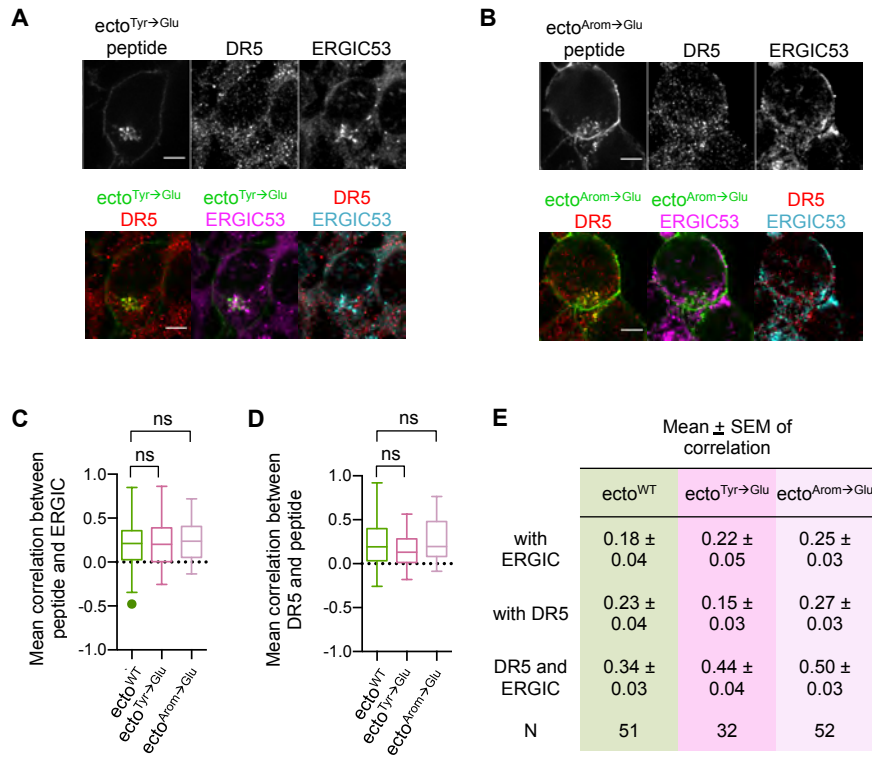


Figure 4—figure supplement 3

